Supporting Information

For

Lanthanide cryptate monometallic coordination complexes

Christian D. Buch, Dmitri Mitcov and Stergios Piligkos

Department of Chemistry, University of Copenhagen, Universitetsparken 5, DK-2100 Copenhagen (Denmark)

E-mail: christian.buch@chem.ku.dk, piligkos@chem.ku.dk

Contents

Infrared spectroscopy

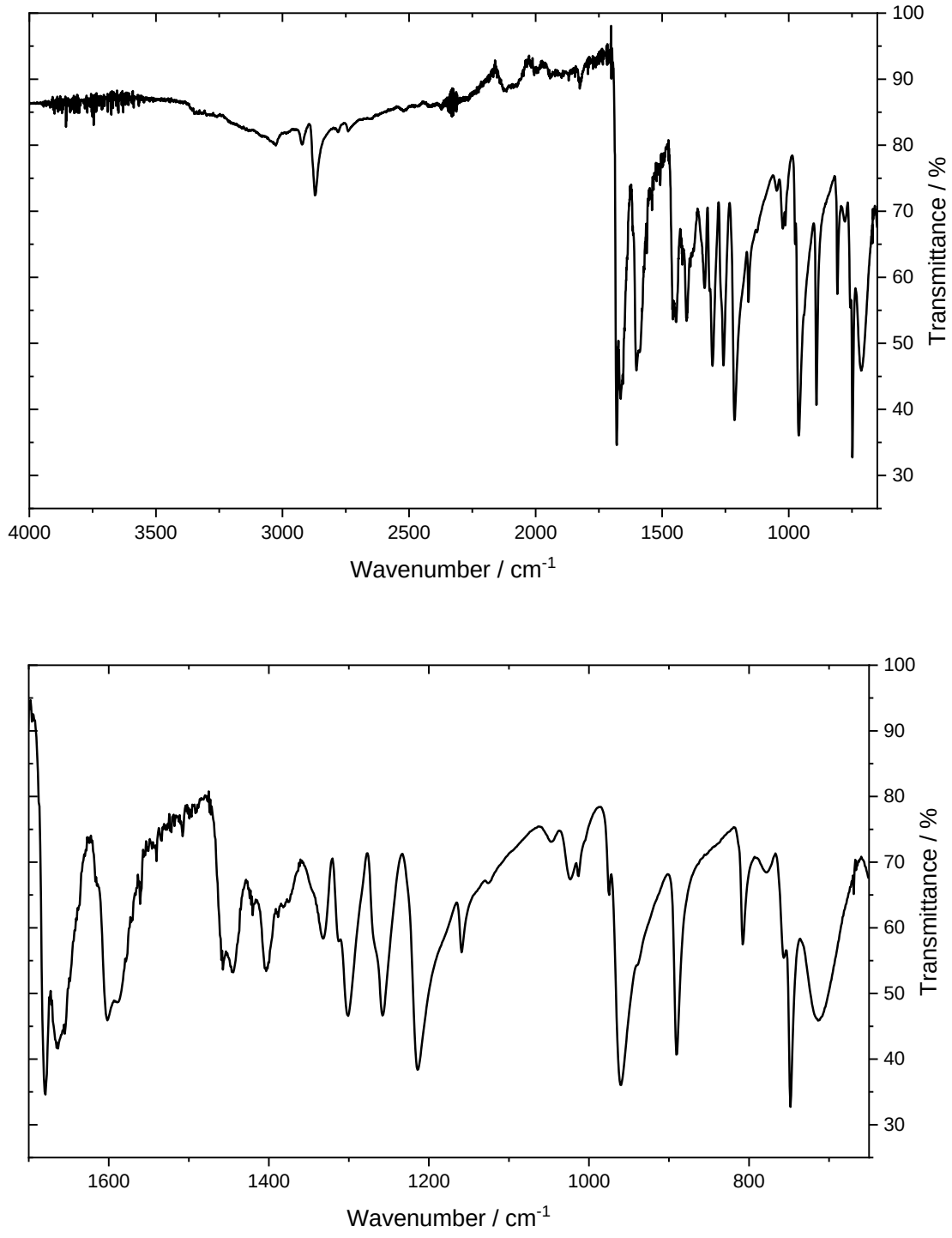

Figure S1 IR spectrum of DFMP (top) with zoom of the 650-1700 cm^{-1} region (bottom)

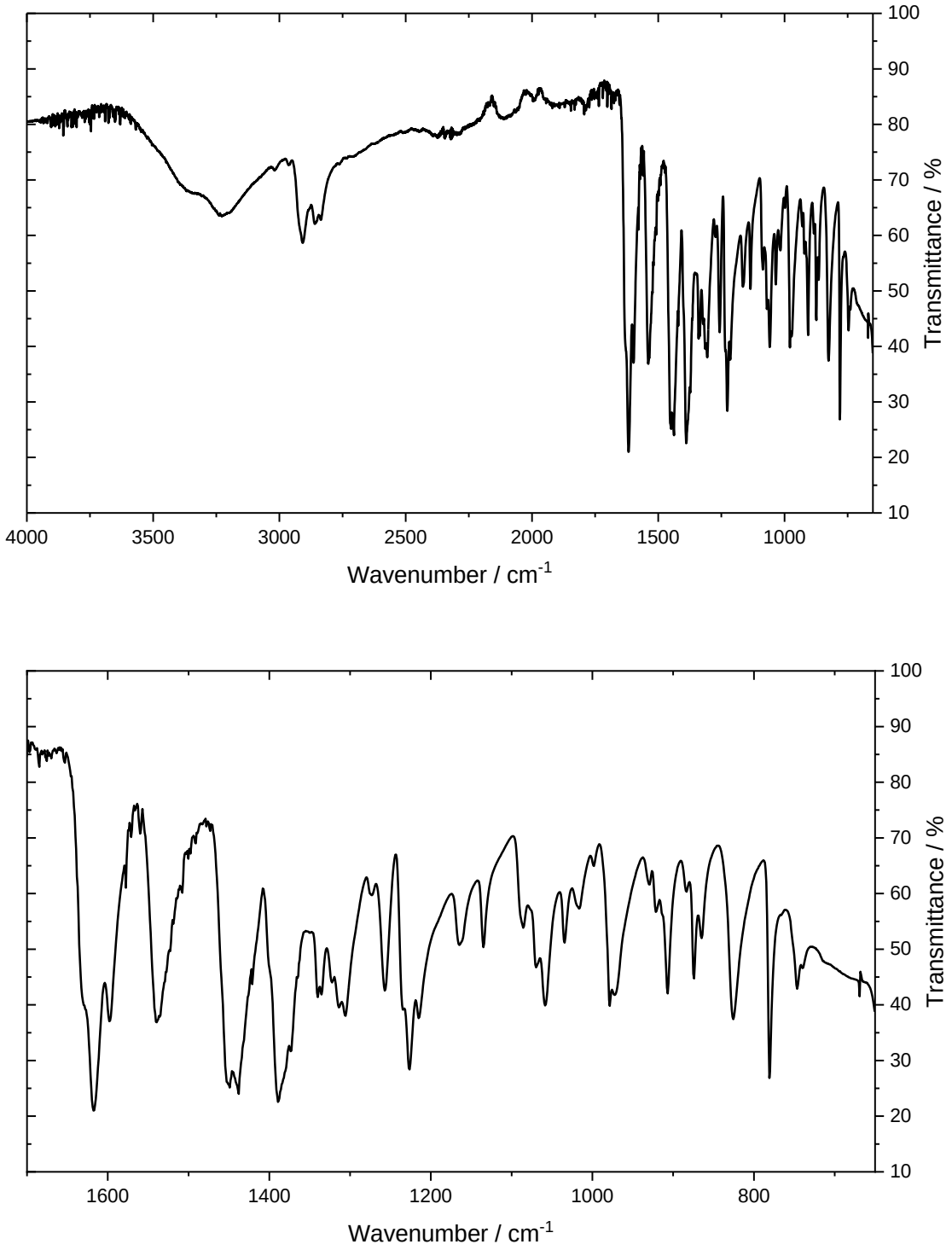

Figure S2 IR spectrum of **1** (top) with zoom of the 650-1700 cm^{-1} region (bottom)

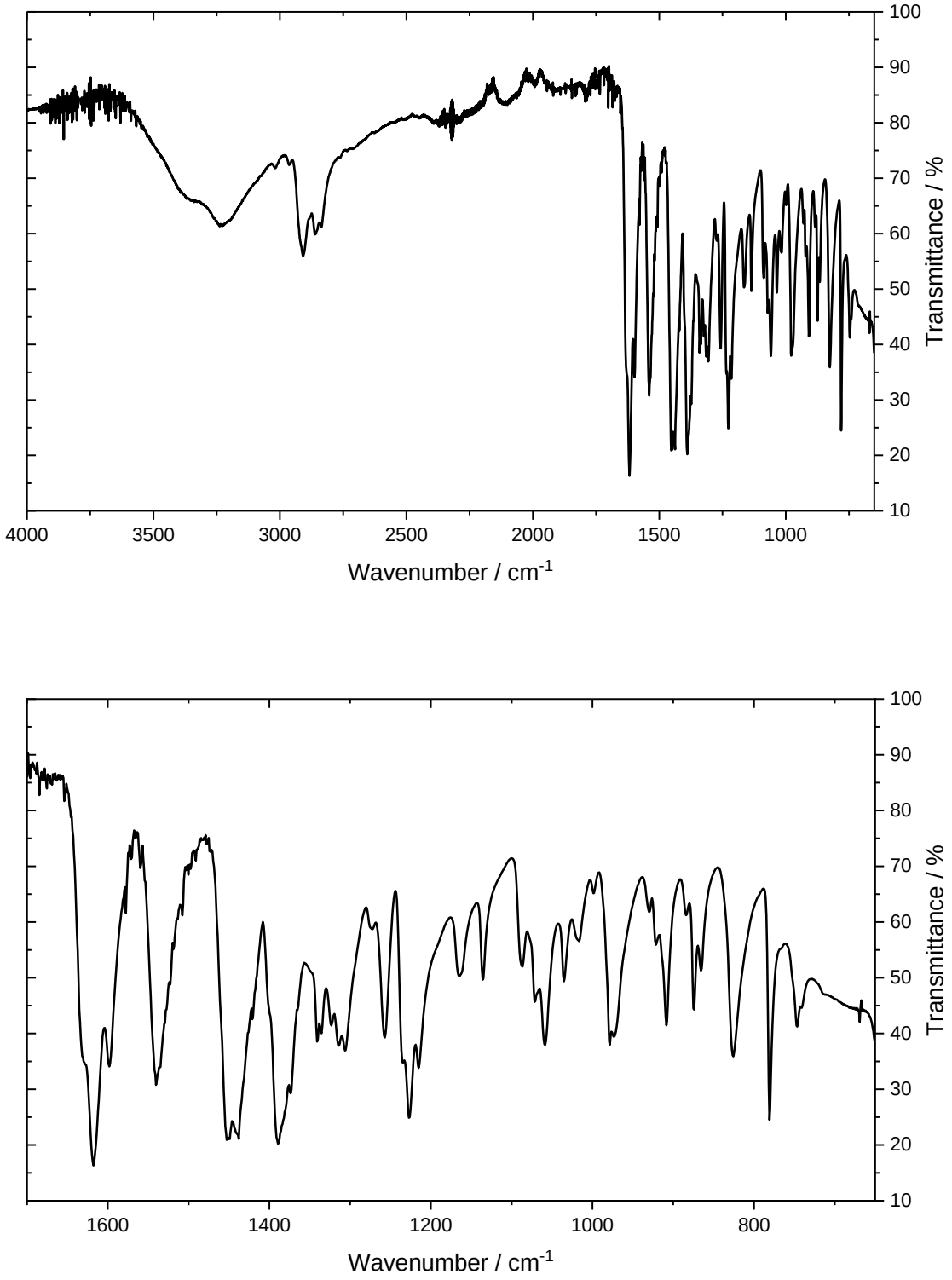

Figure S3 IR spectrum of **2** (top) with zoom of the 650-1700 cm^{-1} region (bottom)

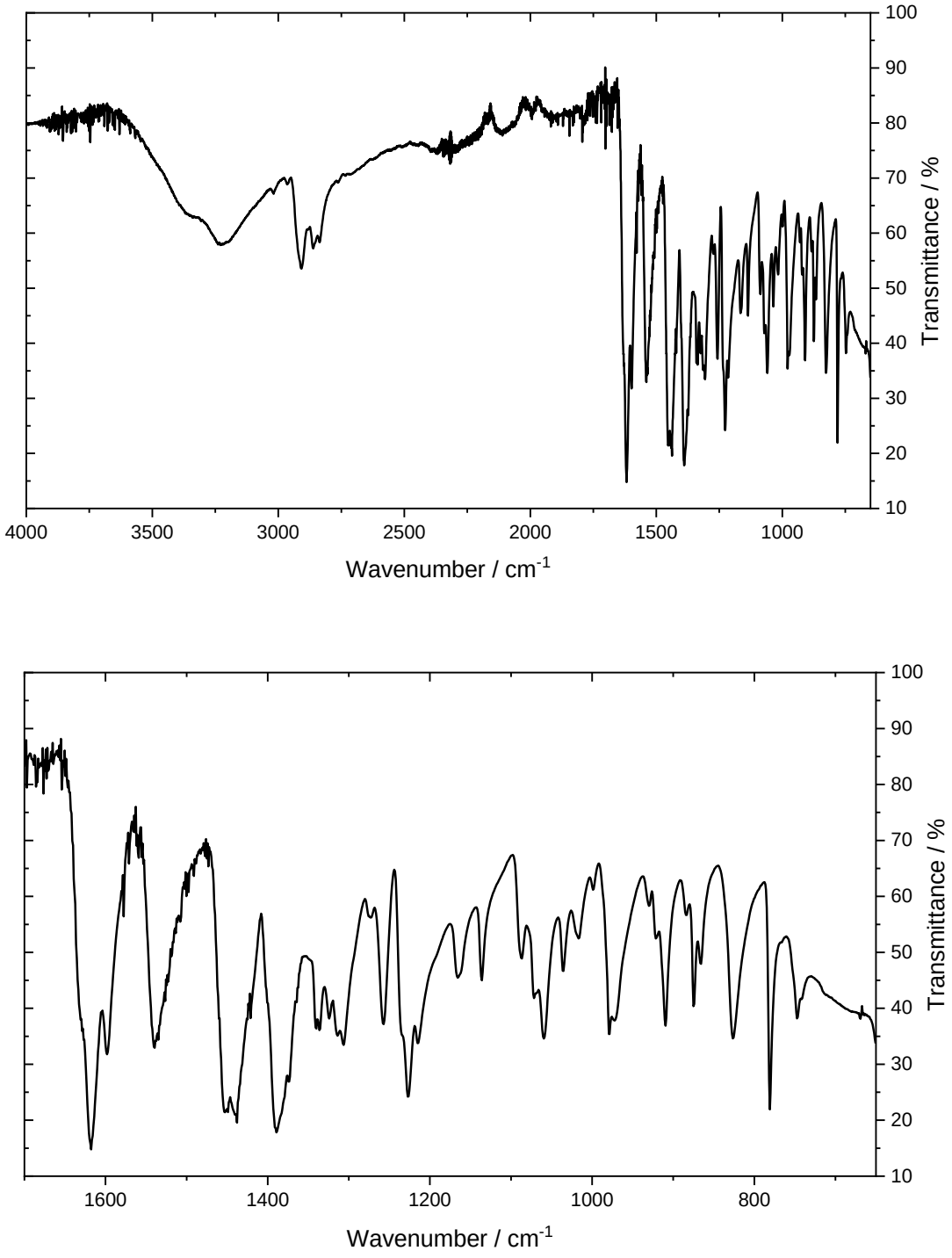

Figure S4 IR spectrum of **3** (top) with zoom of the 650-1700 cm^{-1} region (bottom)

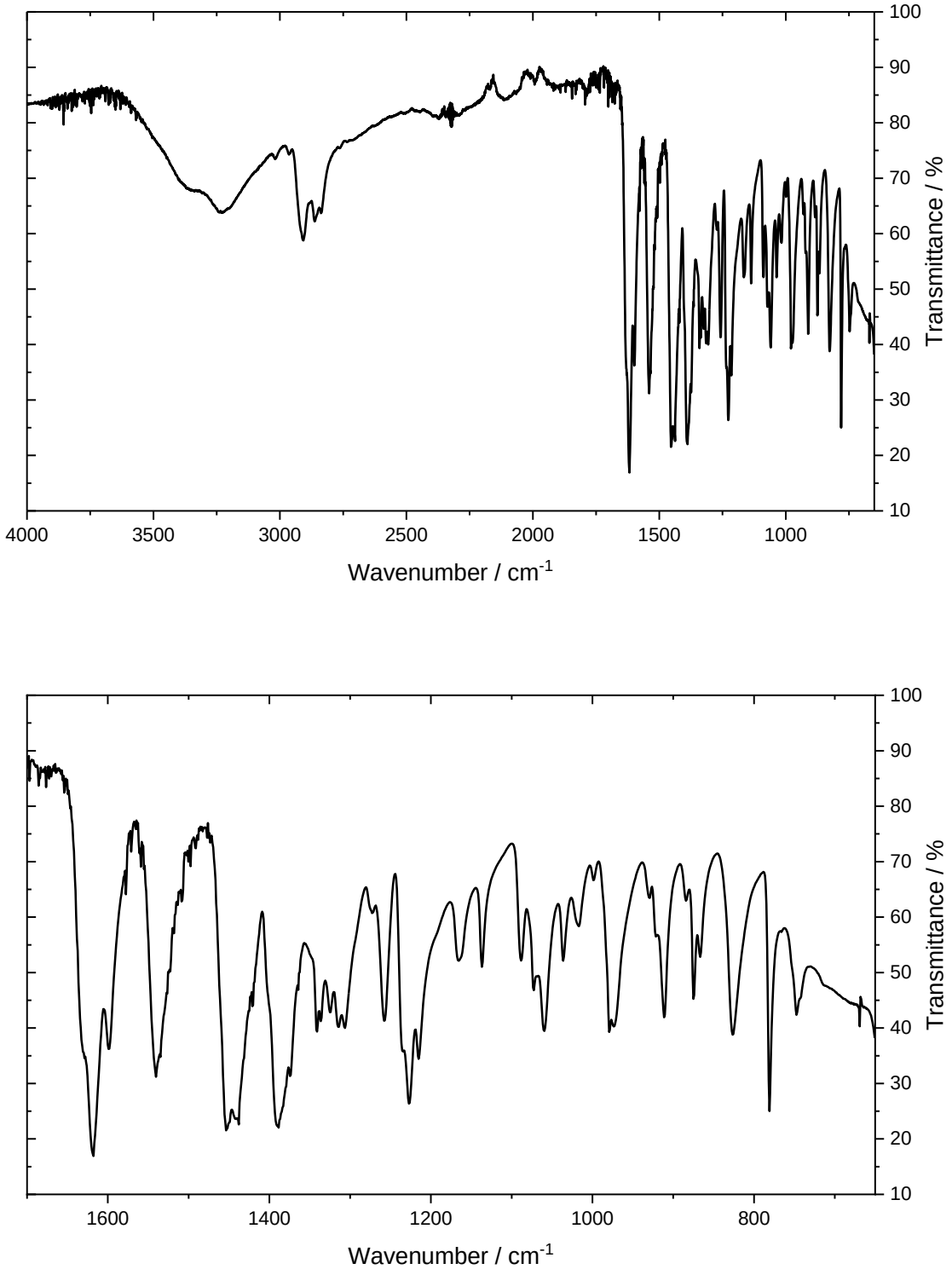

Figure S5 IR spectrum of **4** (top) with zoom of the 650-1700 cm^{-1} region (bottom)

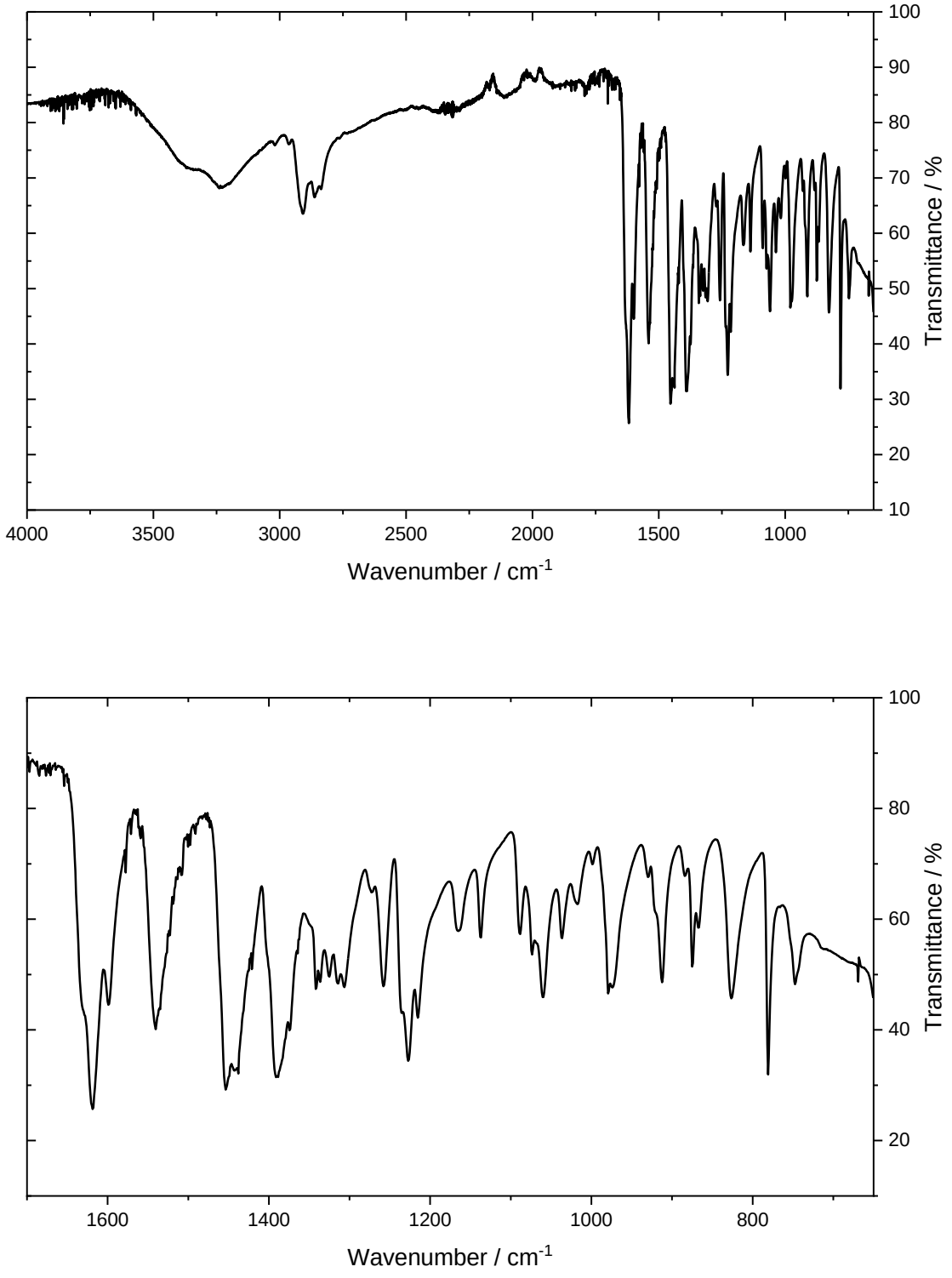

Figure S6 IR spectrum of **5** (top) with zoom of the 650-1700 cm^{-1} region (bottom)

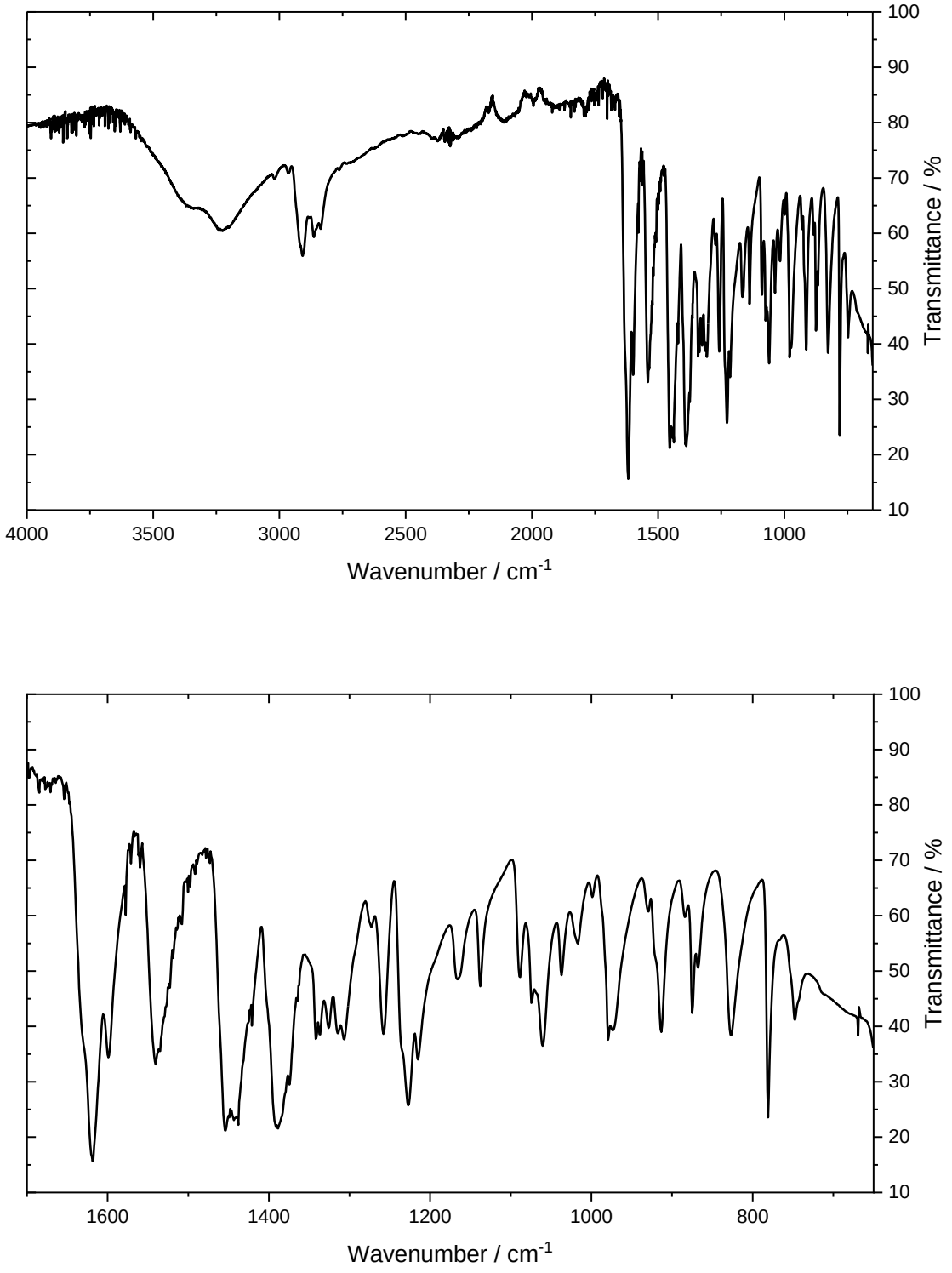

Figure S7 IR spectrum of **6** (top) with zoom of the 650-1700 cm^{-1} region (bottom)

Powder X-ray diffraction

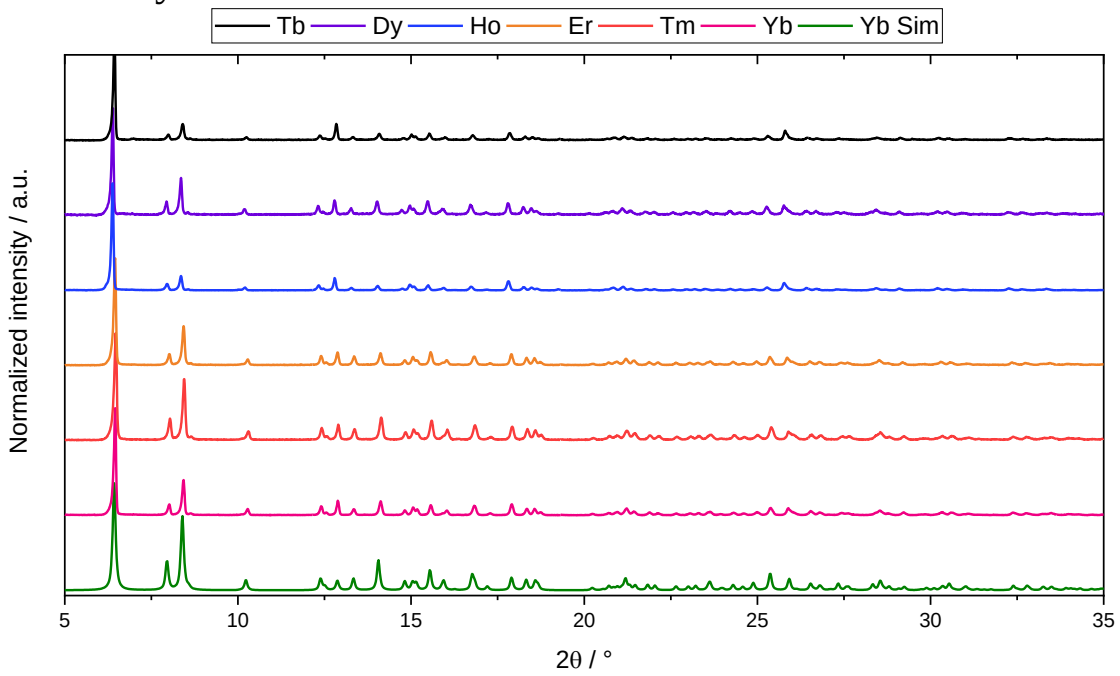

Figure S8 PXRD of **1**-**6** at 300 K. The simulation is based on a crystal structure of **6** measured at room temperature.

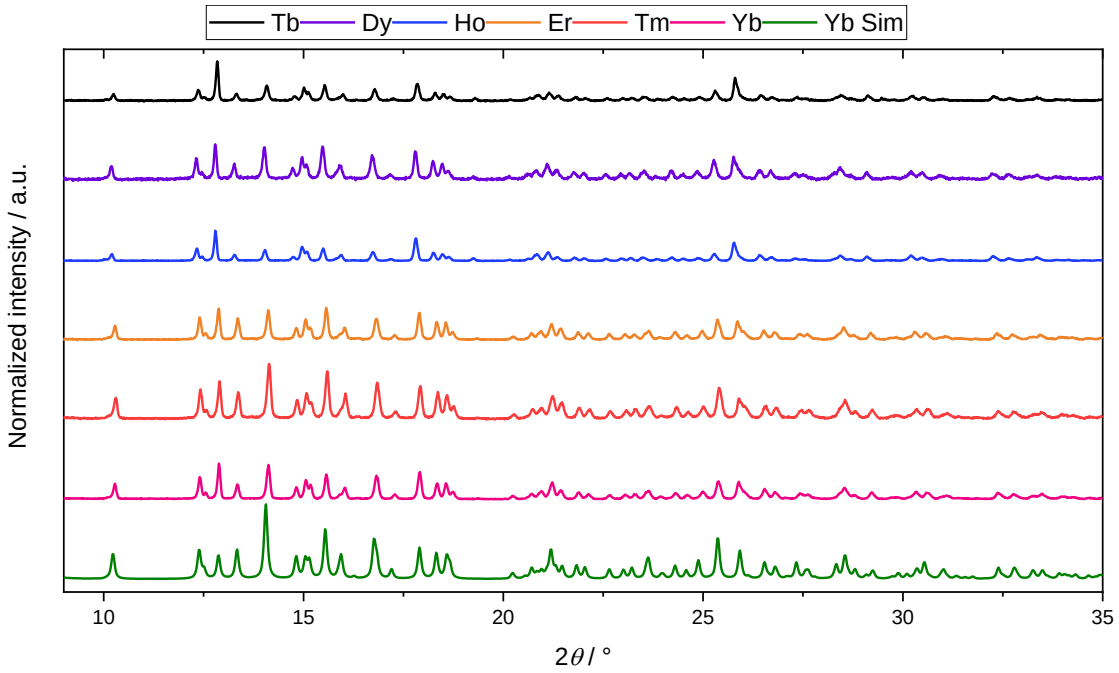

Figure S9 Zoom in on the 2θ = 9 - 35° region of the PXRD data. The simulation is based on a crystal structure of **6** measured at room temperature.

NMR spectra

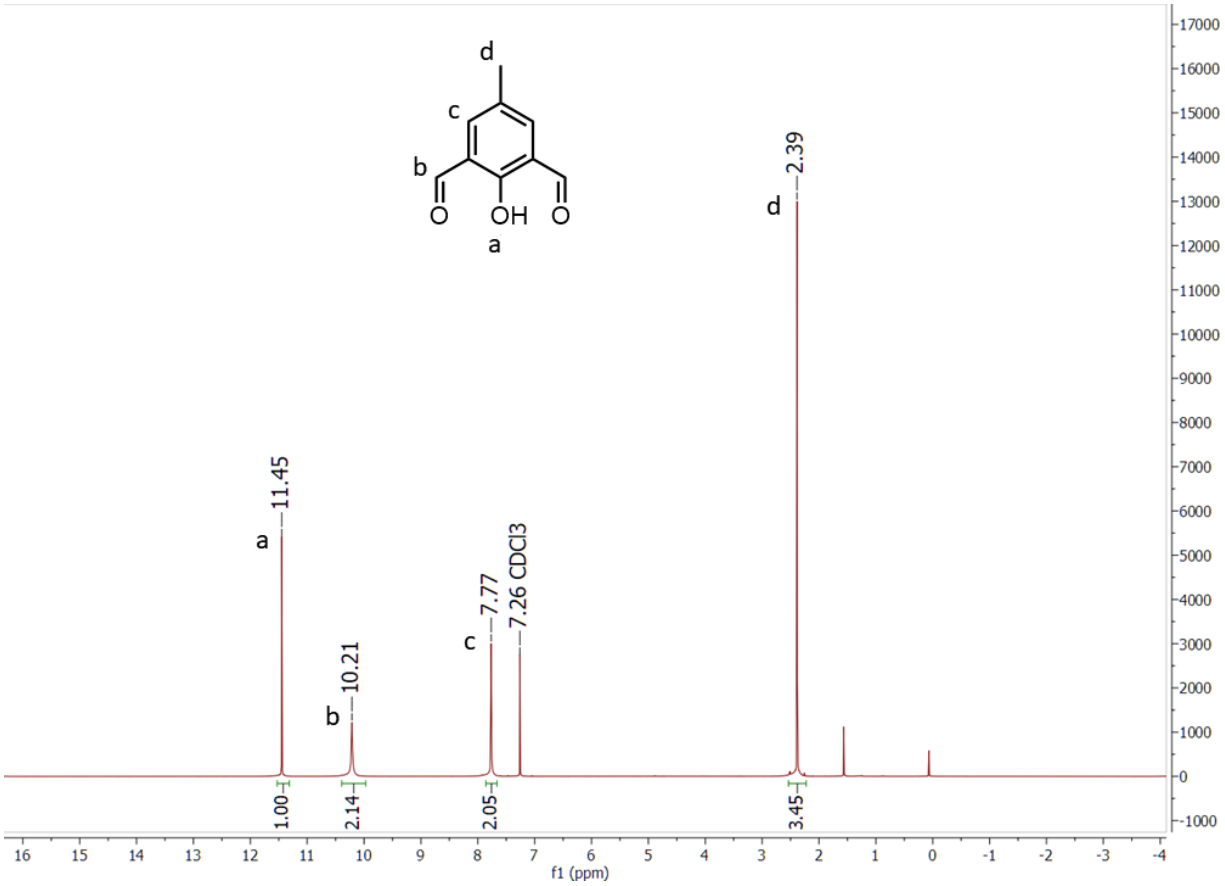

Figure S10 ^{1}H NMR of DFMP in $CDCl_3$. The unassigned peaks at 1.5 and 0 ppm are H_2O and TMS in the chloroform, respectively.[1]

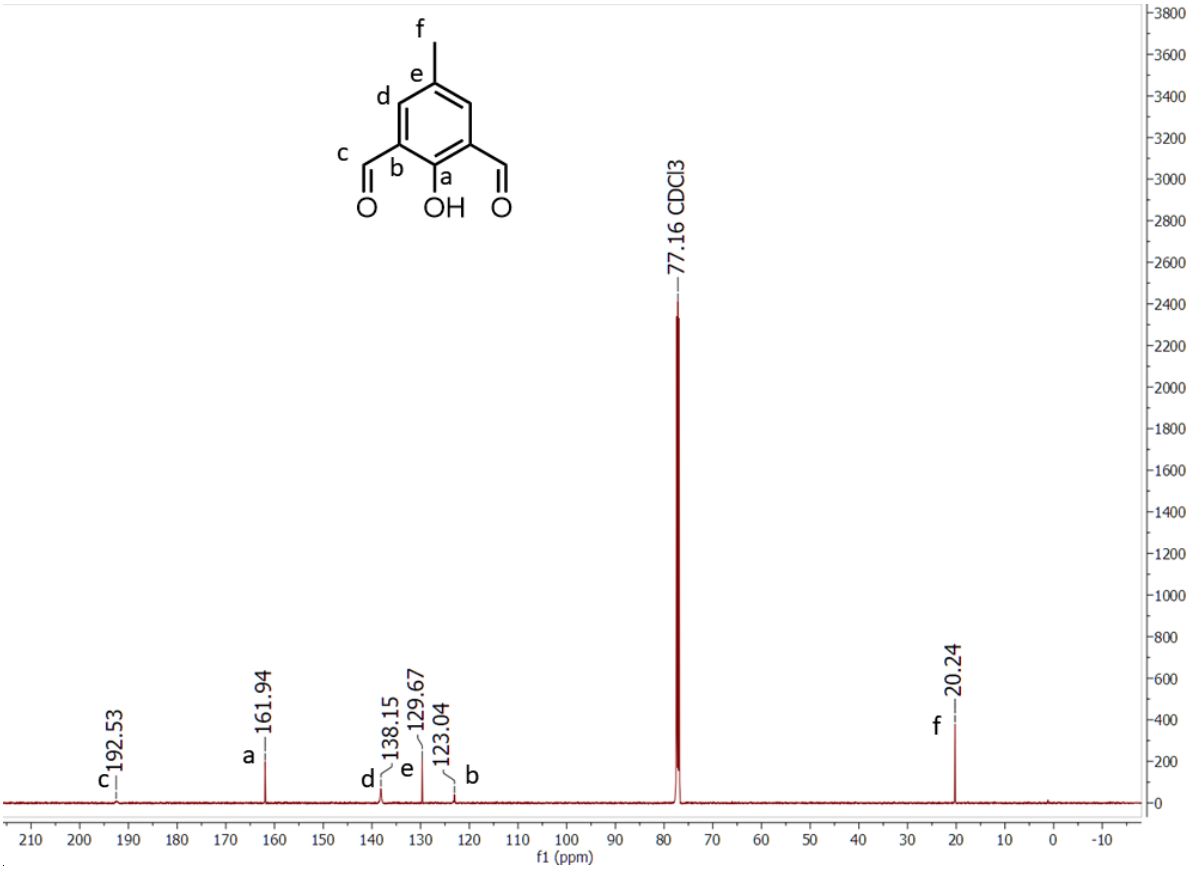

Figure S11 ^{13}C NMR of DFMP in $CDCl_3$.

Mass spectra

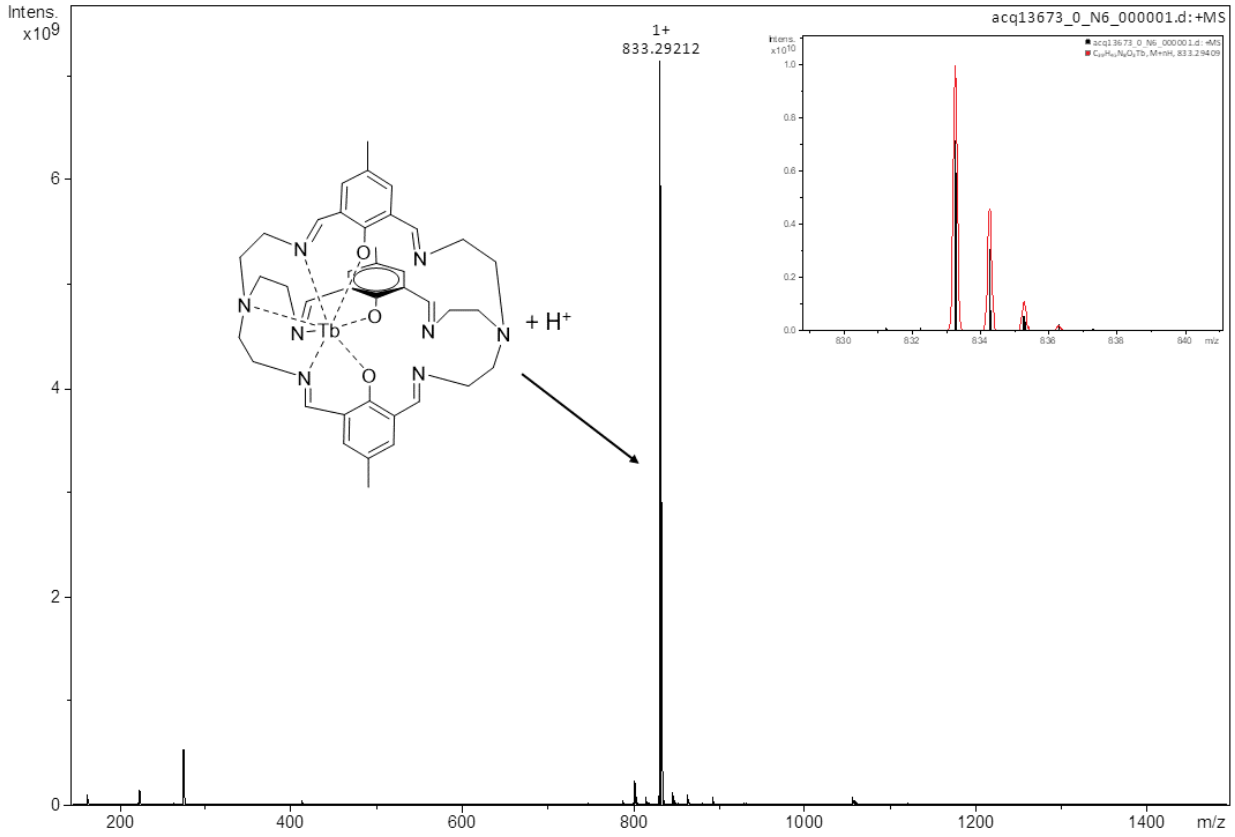

Figure S12 MALDI positive mass spectrum of **1** with insert of signal from the molecular ion (black) with simulated isotope pattern (red)

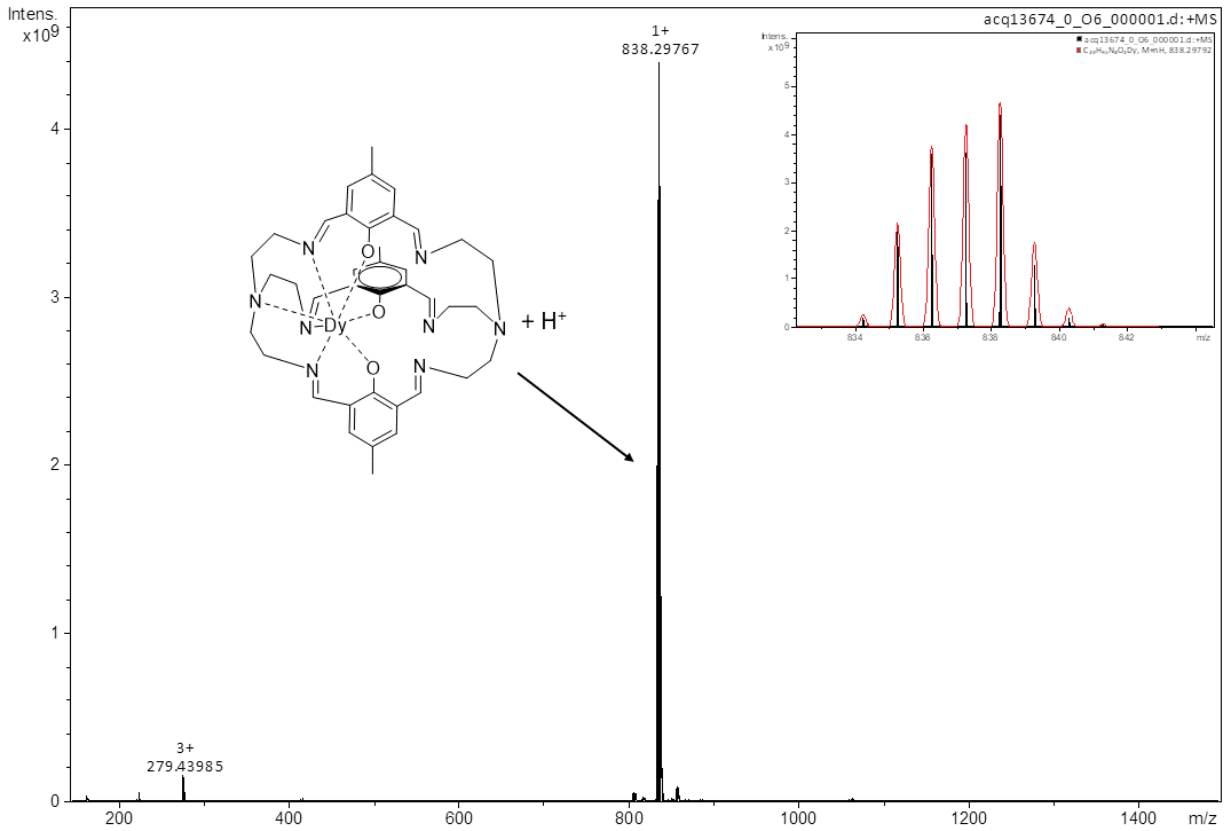

Figure S13 MALDI positive mass spectrum of **2** with insert of signal from the molecular ion (black) with simulated isotope pattern (red)

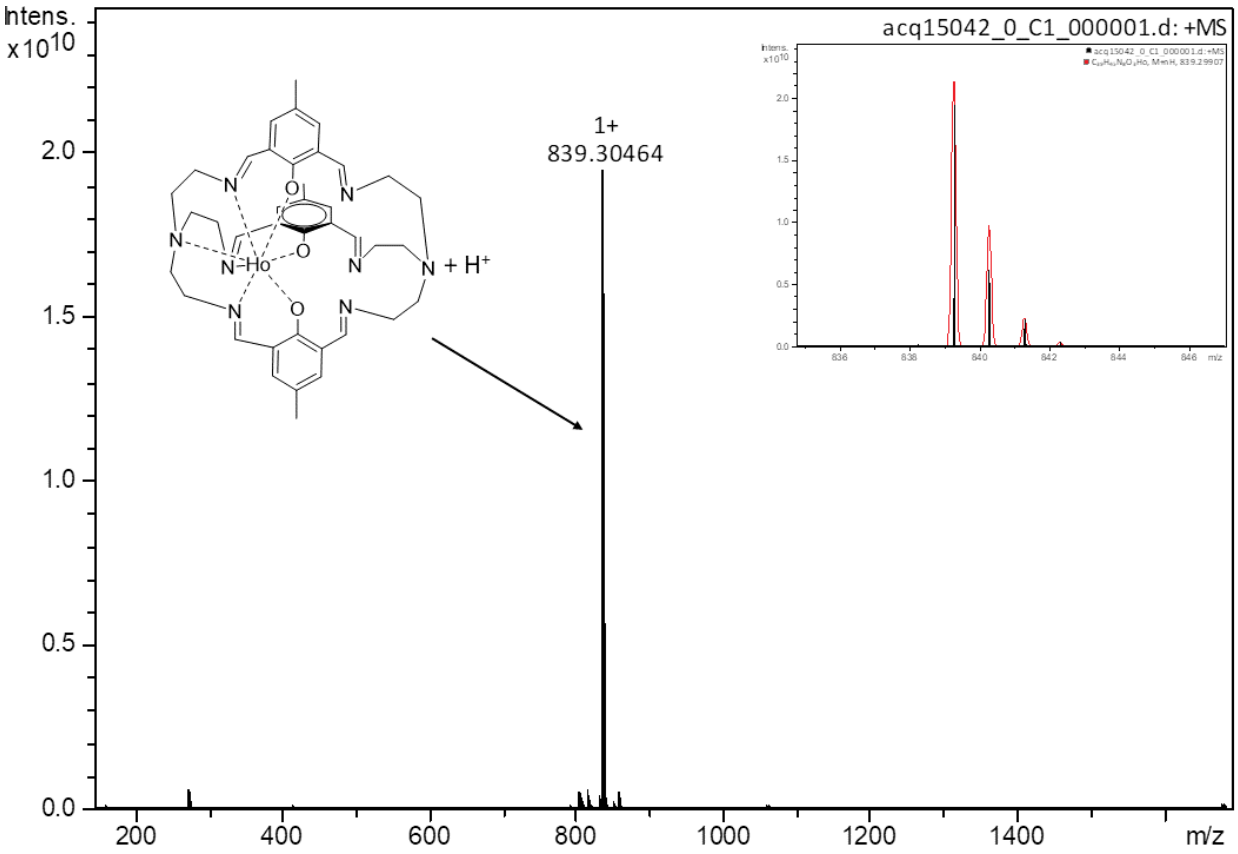

Figure S14 MALDI positive mass spectrum of **3** with insert of signal from the molecular ion (black) with simulated isotope pattern (red)

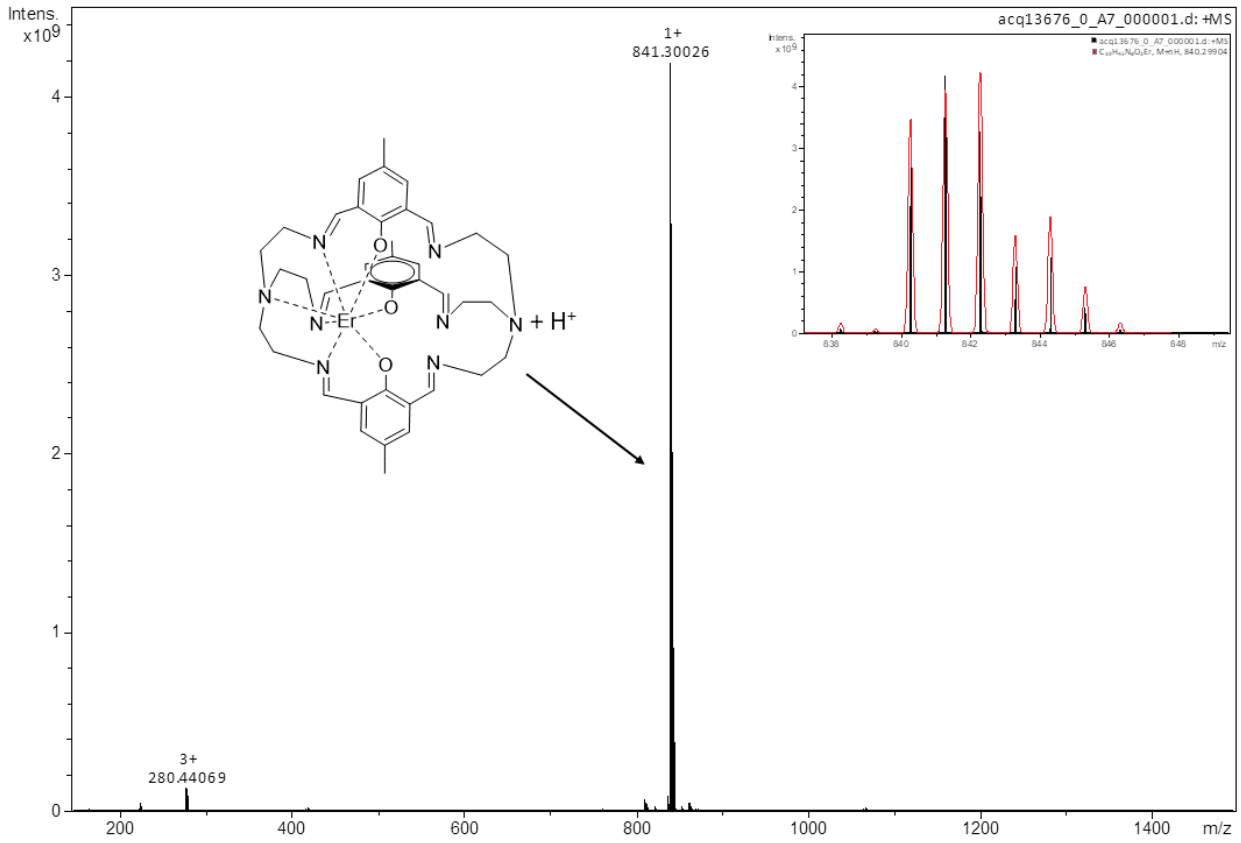

Figure S15 MALDI positive mass spectrum of **4** with insert of signal from the molecular ion (black) with simulated isotope pattern (red)

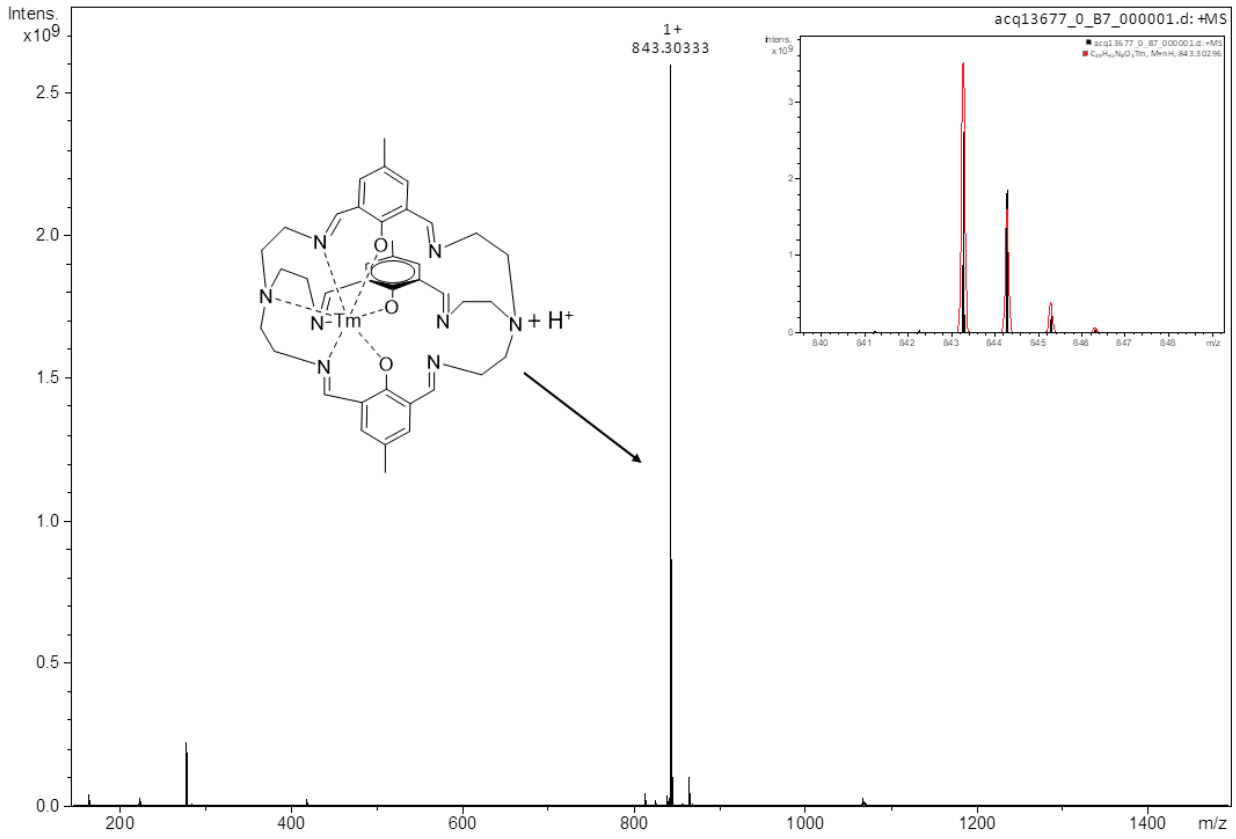

Figure S16 MALDI positive mass spectrum of **5** with insert of signal from the molecular ion (black) with simulated isotope pattern (red)

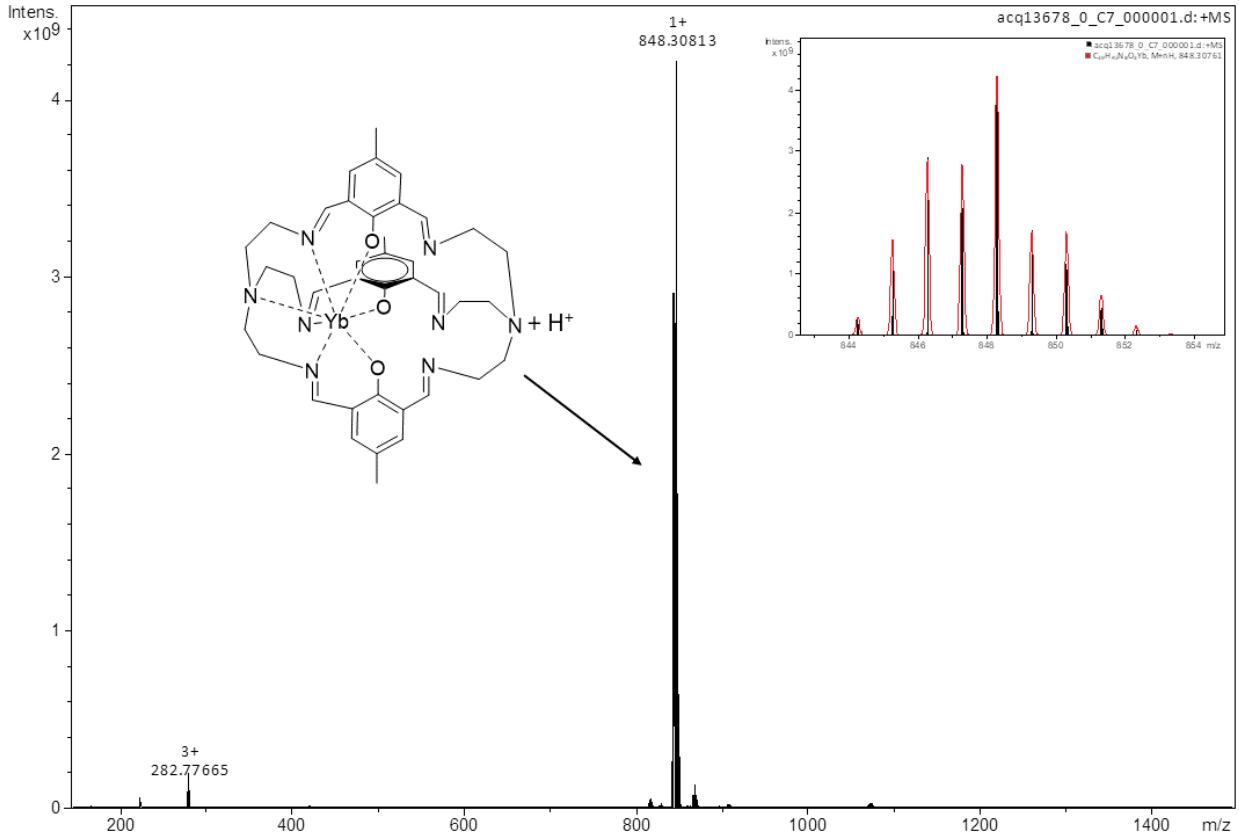

Figure S17 MALDI positive mass spectrum of **6** with insert of signal from the molecular ion (black) with simulated isotope pattern (red)

Variable-temperature-variable-field measurements

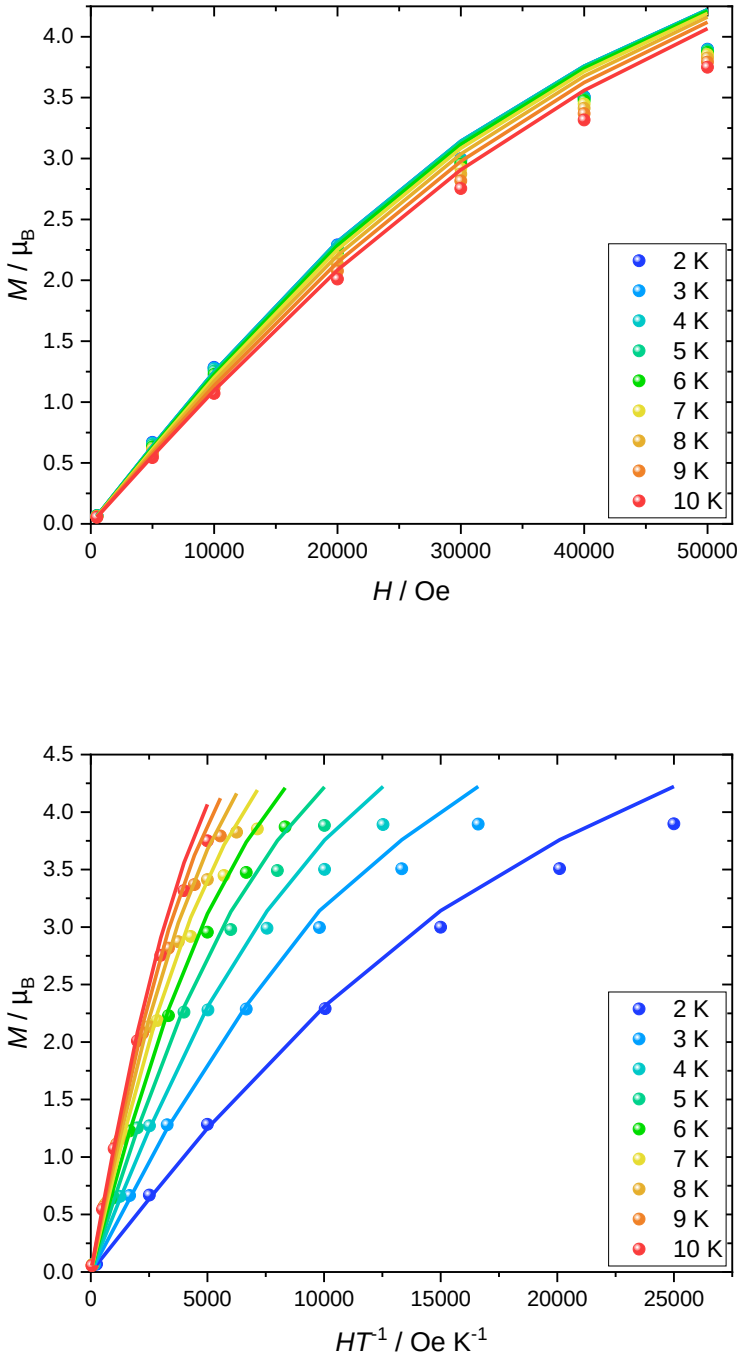

Figure S18 Variable-temperature-variable-field measurements of **1** (top) and reduced magnetisation of **1** (bottom) including the best fit (lines) as described in the main text with the CF parameters found in Table S5.

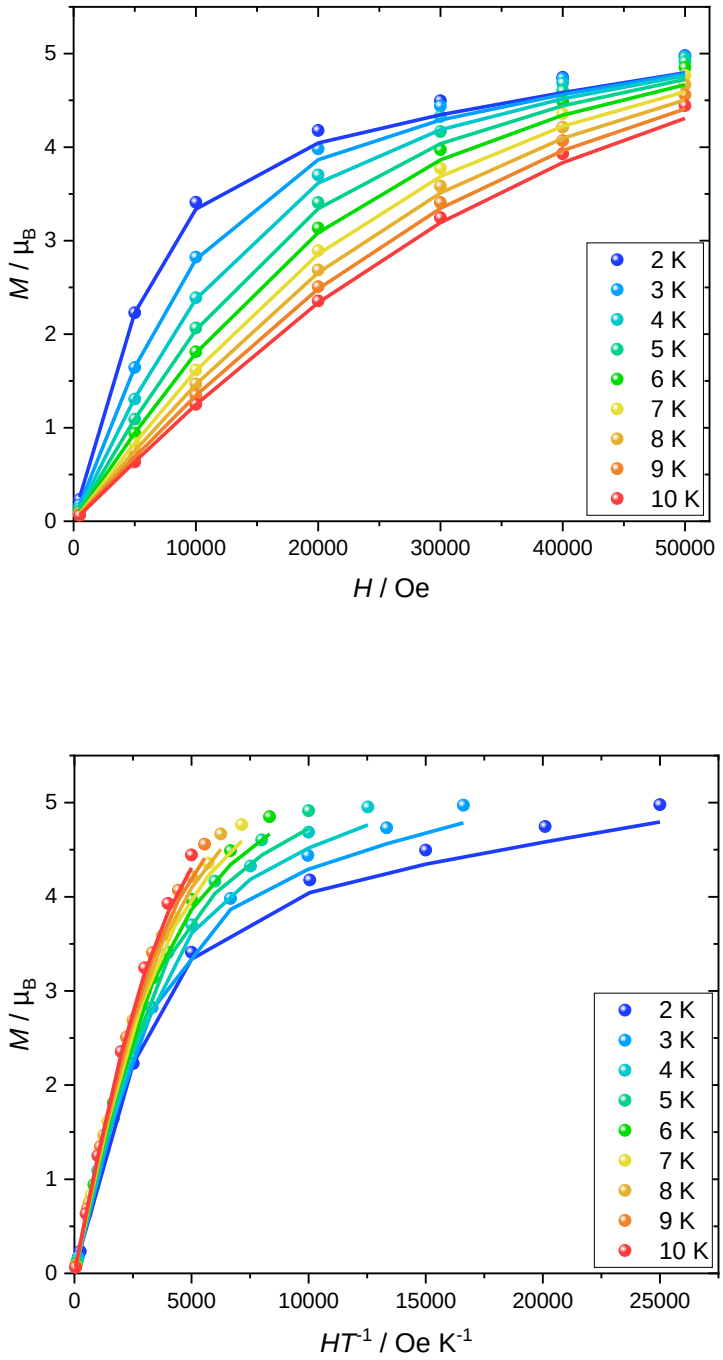

Figure S19 Variable-temperature-variable-field measurements of **2** (top) and reduced magnetisation of **2** (bottom) including the best fit (lines) as described in the main text with the CF parameters found in Table S5.

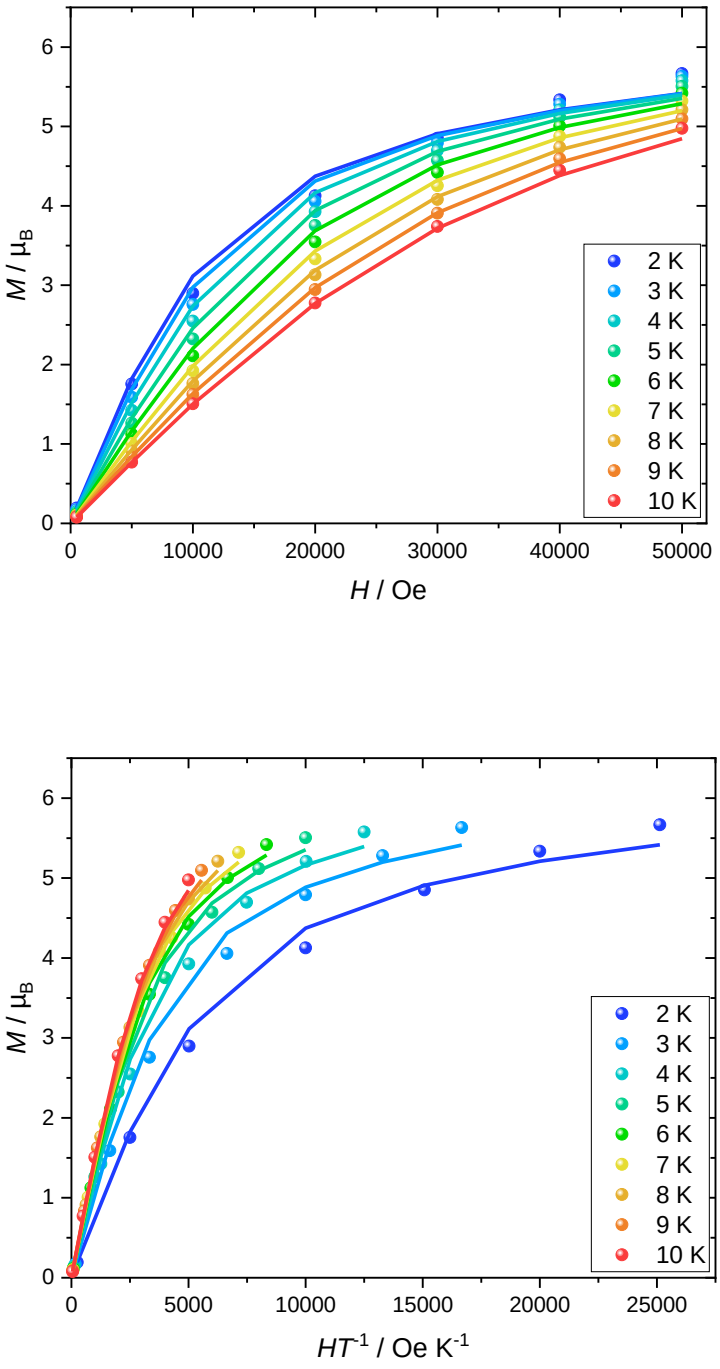

Figure S20 Variable-temperature-variable-field measurements of **3** (top) and reduced magnetisation of **3** (bottom) including the best fit (lines) as described in the main text with the CF parameters found in Table S5.

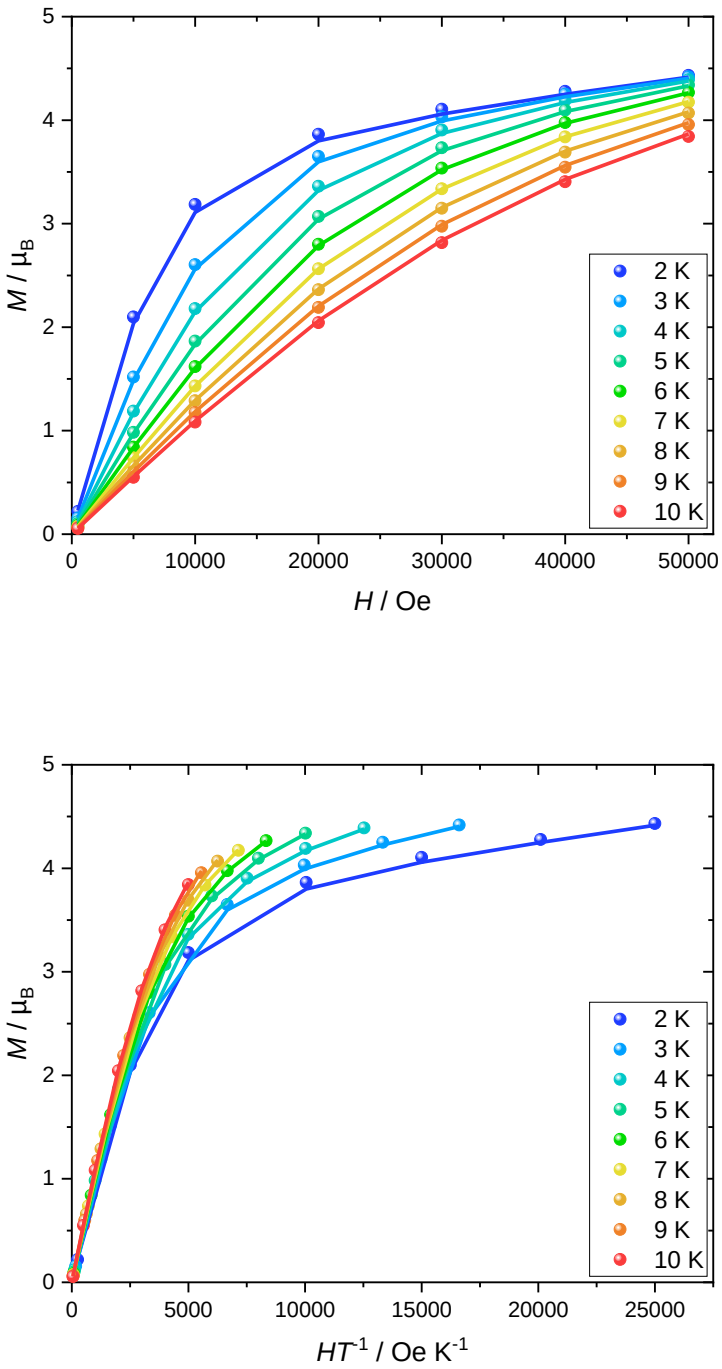

Figure S21 Variable-temperature-variable-field measurements of **4** (top) and reduced magnetisation of **4** (bottom) including the best fit (lines) as described in the main text with the CF parameters found in Table S5.

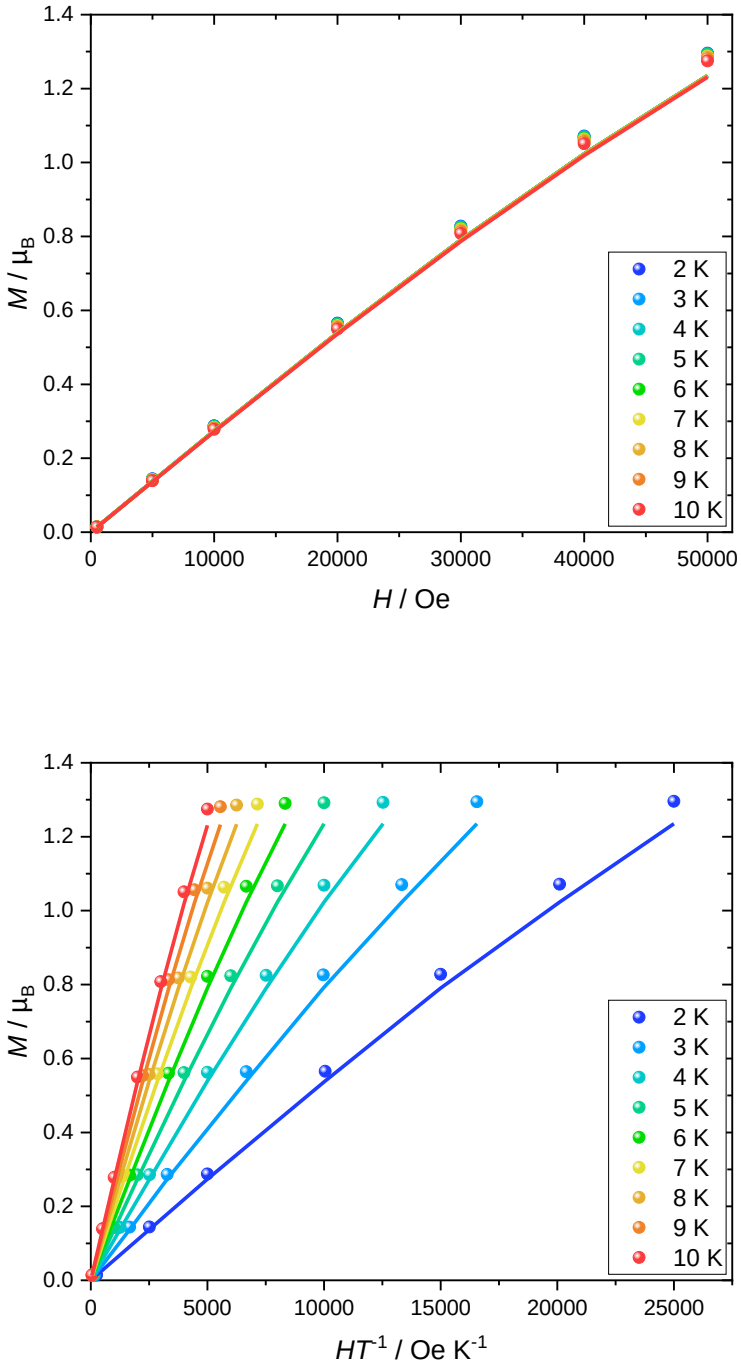

Figure S22 Variable-temperature-variable-field measurements of **5** (top) and reduced magnetisation of **5** (bottom) including the best fit (lines) as described in the main text with the CF parameters found in Table S5.

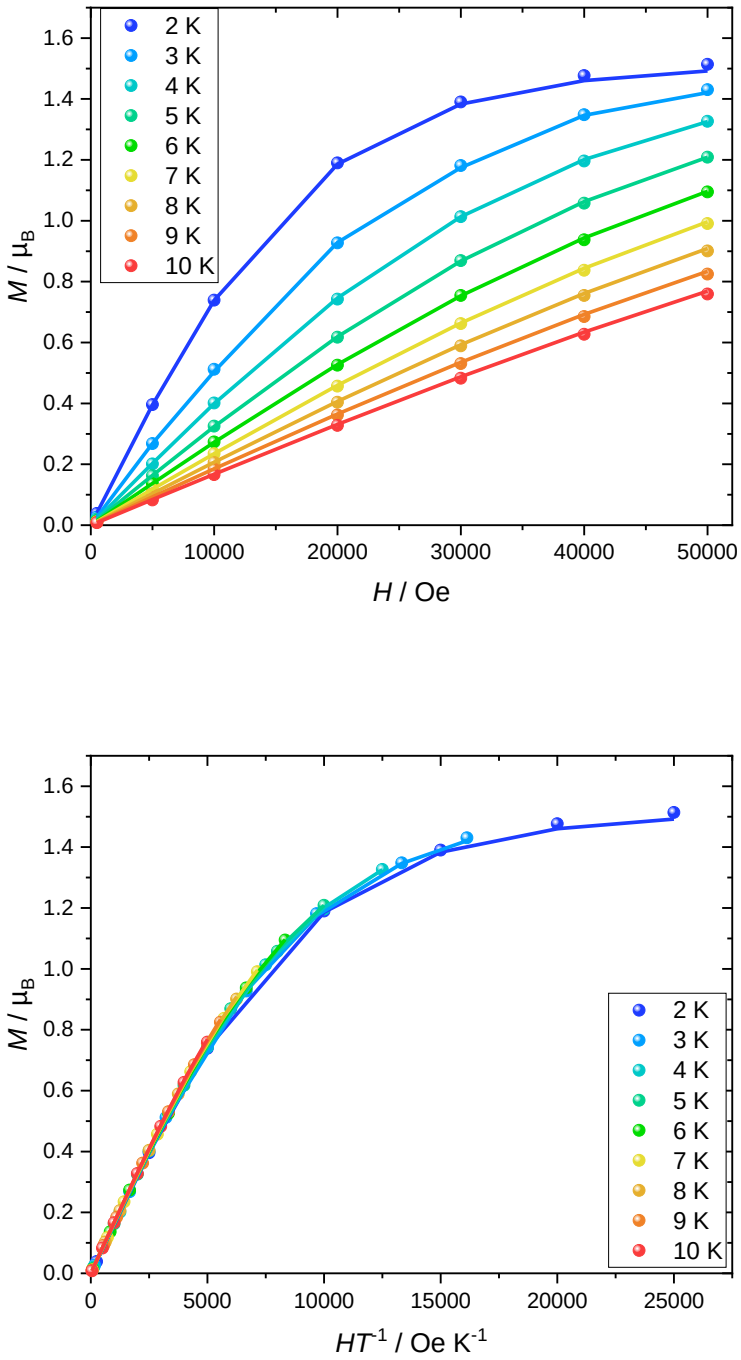

Figure S23 Variable-temperature-variable-field measurements of **6** (top) and reduced magnetisation of **6** (bottom) including the best fit (lines) as described in the main text with the CF parameters found in Table S5.

Modelling using only diagonal terms

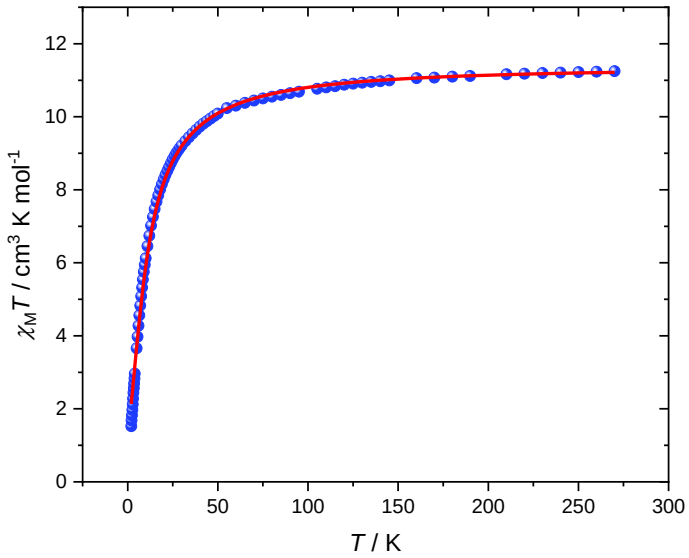

Figure S24 Temperature dependence of the molar χT product of **1** (point) and fit (lines) including only diagonal CF terms as described in the main text. The CF parameters can be found in Table S4**.**

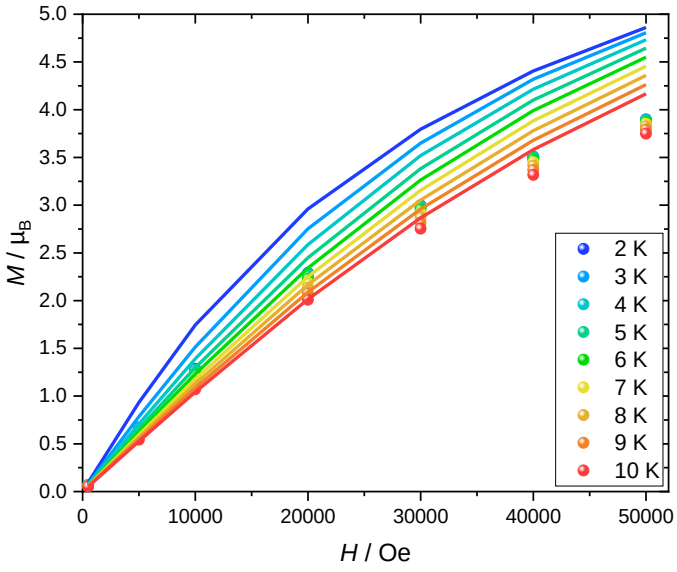

Figure S25 Variable-temperature-variable-field measurements of **1** (points) and best fit (lines) including only diagonal CF terms as described in the main text. The CF parameters can be found in Table S4.

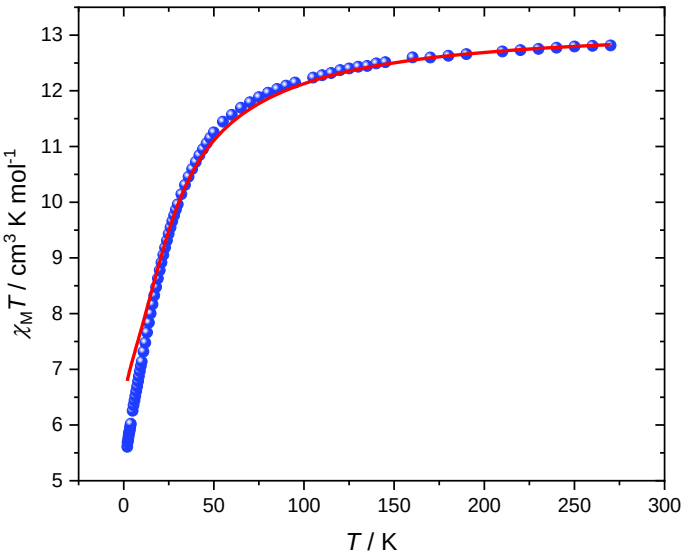

Figure S26 Temperature dependence of the molar χT product of **2** (point) and fit (lines) including only diagonal CF terms as described in the main text. The CF parameters can be found in Table S4**.**

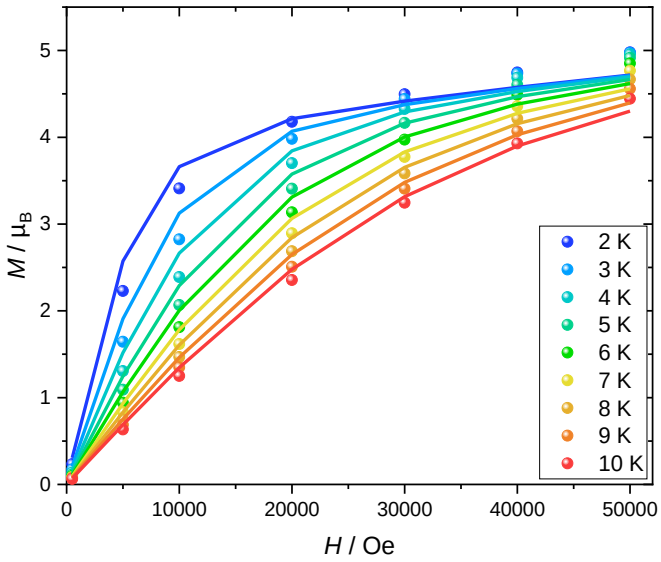

Figure S27 Variable-temperature-variable-field measurements of **2** (points) and best fit (lines) including only diagonal CF terms as described in the main text. The CF parameters can be found in Table S4.

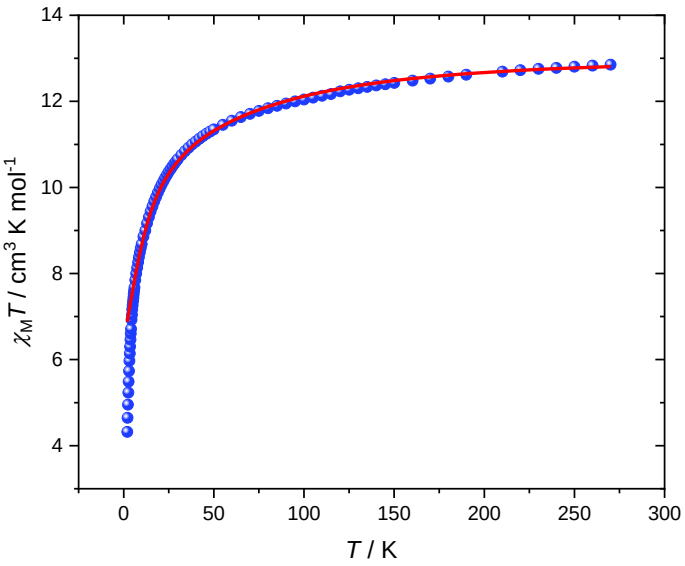

Figure S28 Temperature dependence of the molar χT product of **3** (point) and fit (lines) including only diagonal CF terms as described in the main text. The CF parameters can be found in Table S4**.**

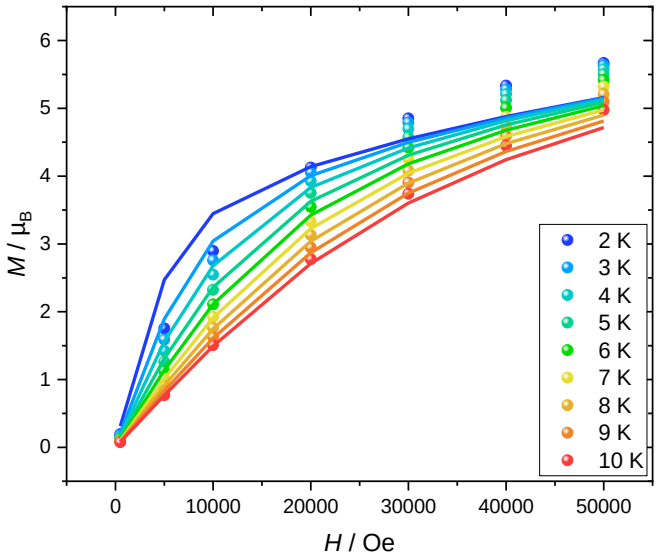

Figure S29 Variable-temperature-variable-field measurements of **3** (points) and best fit (lines) including only diagonal CF terms as described in the main text. The CF parameters can be found in Table S4.

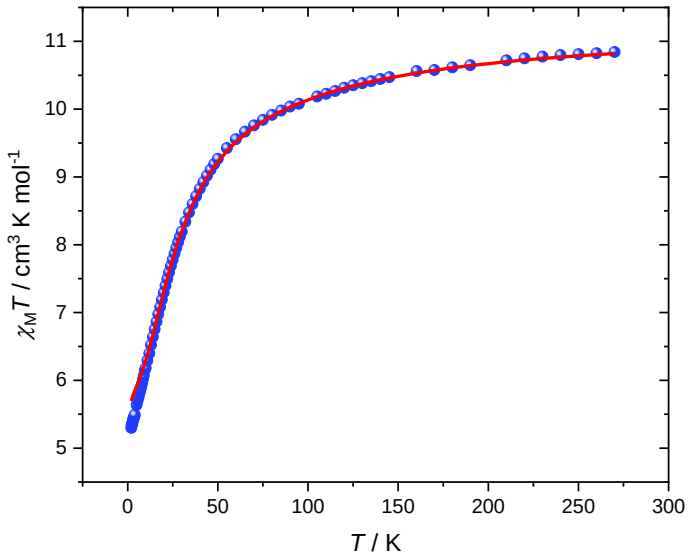

Figure S30 Temperature dependence of the molar χT product of **4** (point) and fit (lines) including only diagonal CF terms as described in the main text. The CF parameters can be found in Table S4**.**

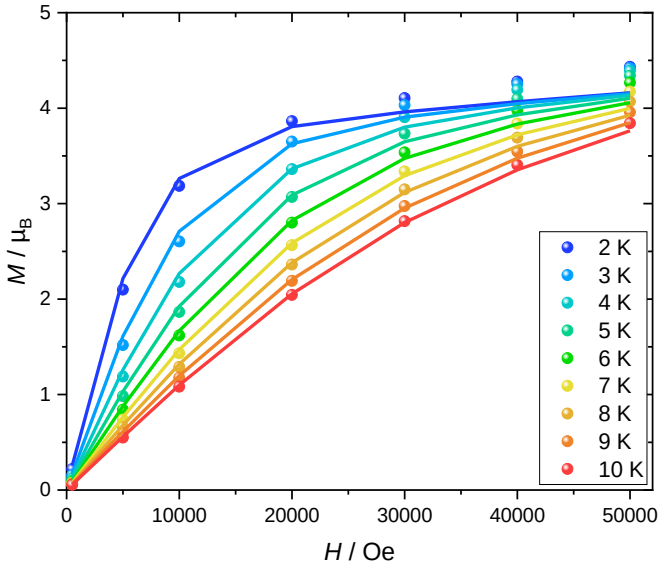

Figure S31 Variable-temperature-variable-field measurements of **4** (points) and best fit (lines) including only diagonal CF terms as described in the main text. The CF parameters can be found in Table S4.

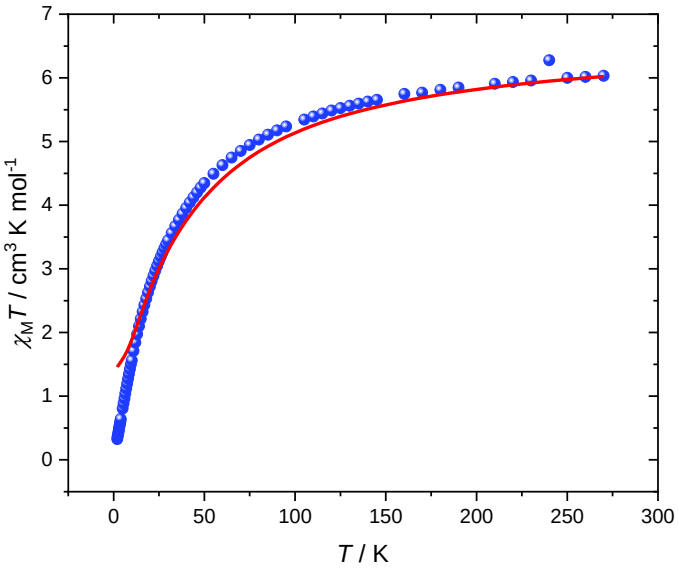

Figure S32 Temperature dependence of the molar χT product of **5** (point) and fit (lines) including only diagonal CF terms as described in the main text. The CF parameters can be found in Table S4**.**

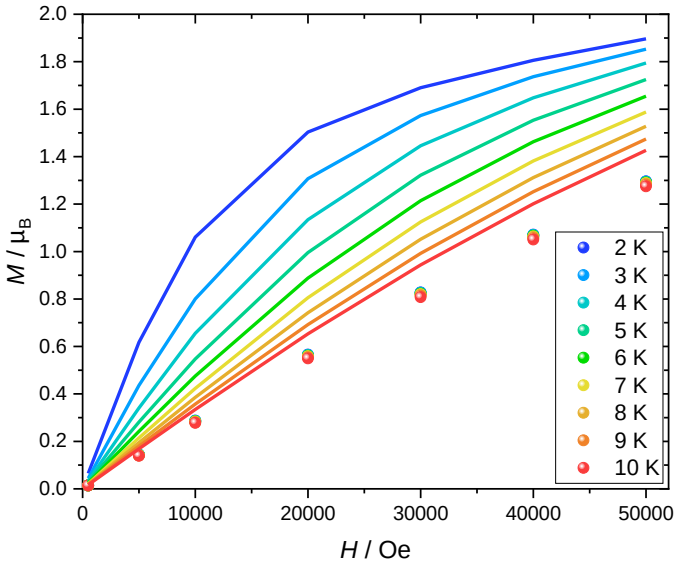

Figure S33 Variable-temperature-variable-field measurements of **5** (points) and best fit (lines) including only diagonal CF terms as described in the main text. The CF parameters can be found in Table S4.

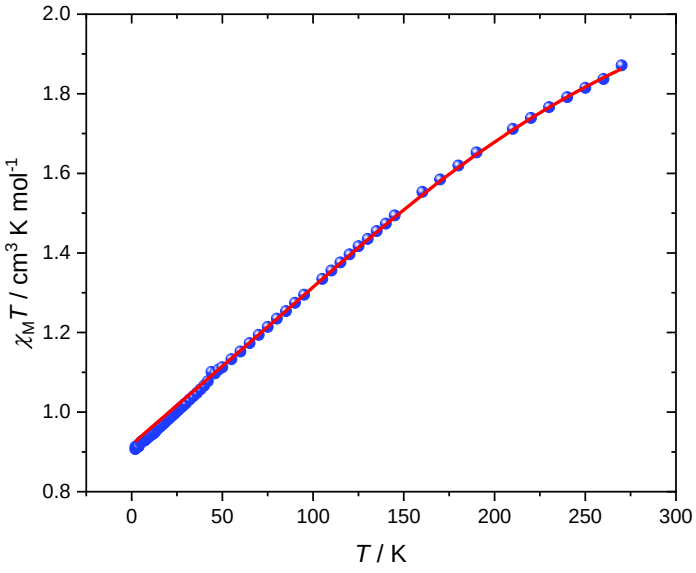

Figure S34 Temperature dependence of the molar χT product of **6** (point) and fit (lines) including only diagonal CF terms as described in the main text. The CF parameters can be found in Table S4**.**

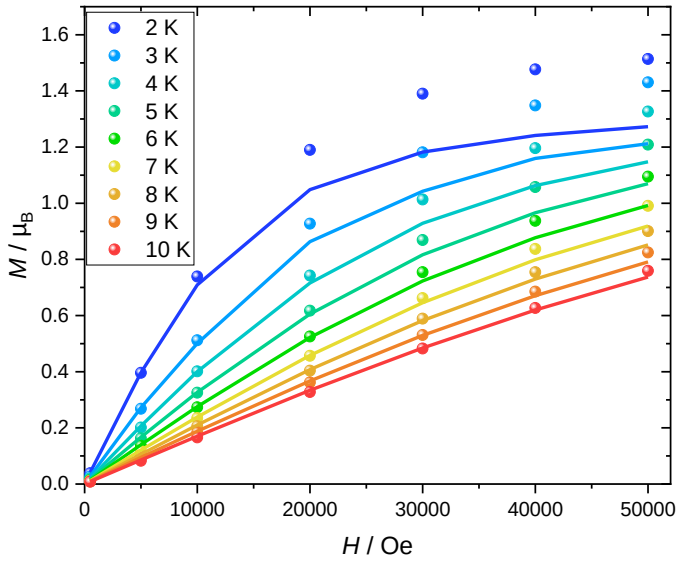

Figure S35 Variable-temperature-variable-field measurements of **5** (points) and best fit (lines) including only diagonal CF terms as described in the main text. The CF parameters can be found in Table S4.

Crystal field parameters

Table S1 Stevens parameters in cm^{-1} for selected Ln(trensal)

Parameters	Tb(trensal)[2]	Dy(trensal)[2]	Ho(trensal)[2]	Er(trensal)[2, 3]	Tm(trensal)[2]	Yb(trensal)[4]
B_2^0	3.12	2.13	0.351	-0.914	-4.81	-11.13
B_4^0	$1.36\cdot10^{-3}$	$1.38\cdot10^{-3}$	$7.74\cdot10^{-4}$	$-2.44\cdot10^{-4}$	$1.75\cdot10^{-3}$	-0.153
B_4^{+3}	0.698	-0.377	-0.188	0.279	0.860	8.92
B_6^{-6}	$-2.83\cdot10^{-4}$	$1.43\cdot10^{-4}$	$-7.00\cdot10^{-4}$	$6.12\cdot10^{-4}$	$6.34\cdot10^{-4}$	0.101
B_6^{-3}	$1.85\cdot10^{-4}$	$3.76\cdot10^{-4}$	$-4.66\cdot10^{-4}$	$-2.44\cdot10^{-4}$	$-1.94\cdot10^{-3}$	0.07
B_6^0	$-1.11\cdot10^{-4}$	$8.03\cdot10^{-5}$	$-9.27\cdot10^{-5}$	$1.28\cdot10^{-4}$	$-4.09\cdot10^{-4}$	$0.71\cdot10^{-2}$
B_6^{+3}	$1.03\cdot10^{-3}$	$-5.82\cdot10^{-4}$	$1.21\cdot10^{-3}$	$-9.36\cdot10^{-4}$	$1.03\cdot10^{-3}$	-0.060
B_6^{+6}	$-1.17\cdot10^{-3}$	$6.49\cdot10^{-4}$	$-5.65\cdot10^{-4}$	$1.07\cdot10^{-3}$	$-4.27\cdot10^{-3}$	0.034

Table S2 Stevens parameters in cm^{-1} for **1**-**6** obtained as the best fit to the χT product and variable-temperature-variable-field measurements setting the off-diagonal CF parameters to 0 and only modelling using the diagonal parameters as described in the main text

Parameters	**1**	**2**	**3**	**4**	**5**	**6**
B_2^0	3.10	2.13	0.345	-0.769	-2.00	-11.28
B_4^0	$-3.73\cdot10^{-3}$	$8.21\cdot10^{-3}$	$8.58\cdot10^{-3}$	$-1.24\cdot10^{-2}$	$6.25\cdot10^{-3}$	0.313
B_6^0	$-2.66\cdot10^{-4}$	$1.39\cdot10^{-4}$	$6.84\cdot10^{-5}$	$1.15\cdot10^{-4}$	$-8.19\cdot10^{-4}$	$2.10\cdot10^{-2}$

Table S3 Stevens parameters in cm^{-1} for **1-6** obtained as the best fit to the χT product and field-dependent magnetisation measurements fixing the off-diagonal CF parameters to those of the corresponding Ln(trensal) complex as described in the main text. Fit parameters are in bold.

Parameters	**1**	**2**	**3**	**4**	**5**	**6**
$\boldsymbol{B_2^0}$	**4.22**	**3.38**	**2.16**	**-0.913**	**-3.50**	**-7.86**
$\boldsymbol{B_4^0}$	$\mathbf{6.53\cdot10^{-5}}$	$\mathbf{9.64\cdot10^{-3}}$	$\mathbf{8.59\cdot10^{-3}}$	$\mathbf{-3.22\cdot10^{-3}}$	$\mathbf{2.10\cdot10^{-8}}$	$\mathbf{-2.52\cdot10^{-2}}$
B_4^{+3}	0.698	-0.377	-0.188	0.279	0.860	8.92
B_6^{-6}	$-2.83\cdot10^{-4}$	$1.43\cdot10^{-4}$	$-7.00\cdot10^{-4}$	$6.12\cdot10^{-4}$	$6.34\cdot10^{-4}$	0.101
B_6^{-3}	$1.85\cdot10^{-4}$	$3.76\cdot10^{-4}$	$-4.66\cdot10^{-4}$	$-2.44\cdot10^{-4}$	$-1.94\cdot10^{-3}$	0.07
$\boldsymbol{B_6^0}$	$\mathbf{-4.55\cdot10^{-5}}$	$\mathbf{1.29\cdot10^{-4}}$	$\mathbf{-9.89\cdot10^{-6}}$	$\mathbf{6.25\cdot10^{-8}}$	$\mathbf{2.47\cdot10^{-4}}$	$\mathbf{6.28\cdot10^{-5}}$
B_6^{+3}	$1.03\cdot10^{-3}$	$-5.82\cdot10^{-4}$	$1.21\cdot10^{-3}$	$-0.936\cdot10^{-3}$	$1.03\cdot10^{-3}$	-0.060
B_6^{+6}	$-1.17\cdot10^{-3}$	$6.49\cdot10^{-4}$	$-5.65\cdot10^{-4}$	$1.07\cdot10^{-3}$	$-4.27\cdot10^{-3}$	0.034

Conversion of CF parameters from Wybourne to Stevens formalism

The CF parameters of Ln(trensal) determined by Riley *et al.*[2, 3] are given within the Wybourne formalism. In this work we use the Stevens formalism, since we only interpret ground term properties, as we have not conducted optical spectroscopy studies that are outside the scope of this study.

In order to convert the Wybourne crystal field parameters, $B_q^k(W)$ to Stevens crystal field parameters, $B_k^q(S)$, we use the definition of these latter as[5]:

$$B_k^q(S) = \langle J\|(\alpha,\beta,\gamma)\|J\rangle\, A_k^q\, \langle r^k\rangle$$

with $\langle J\|(\alpha,\beta,\gamma)\|J\rangle$ reduced matrix elements, depending thus only on the tensor rank k ($\langle J\|\alpha\|J\rangle$, $\langle J\|\beta\|J\rangle$ and $\langle J\|\gamma\|J\rangle$ for $k = 2$, $k = 4$ and $k = 6$, respectively) and the relation

$$B_q^k(W) = c_{k,q}\, A_k^q\, \langle r^k\rangle$$

from Table 6, page 171 in Handbook on The Physics and Chemistry of Rare Earths.[6]

Thus:

$$B_k^q(S) = \frac{B_q^k(W)\cdot\langle J\|(\alpha,\beta,\gamma)\|J\rangle}{c_{k,q}}$$

The numerical values of $\langle J\|\alpha\|J\rangle$, $\langle J\|\beta\|J\rangle$ and $\langle J\|\gamma\|J\rangle$ are found in Table 20, page 874-875 in Abragam and Bleaney.[5]

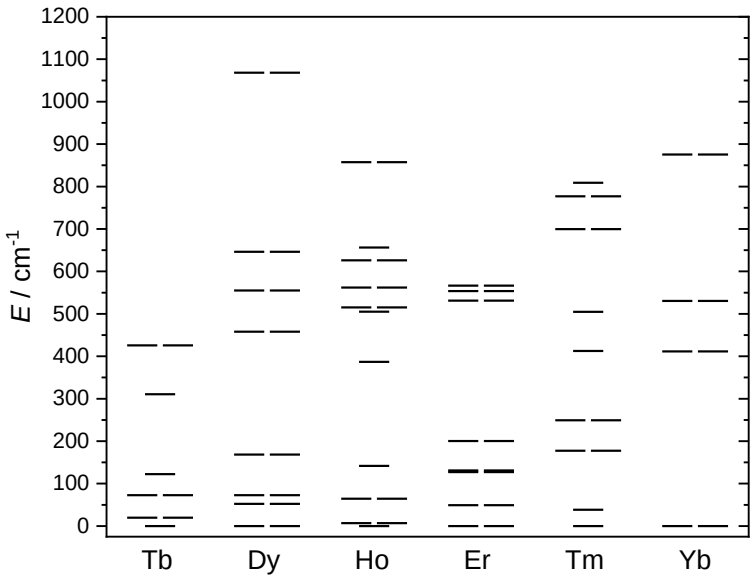

Figure S36 Energy level splitting of the ground multiplet in **1**-**6**. The energy levels are determined using the CF parameters in Table S3.

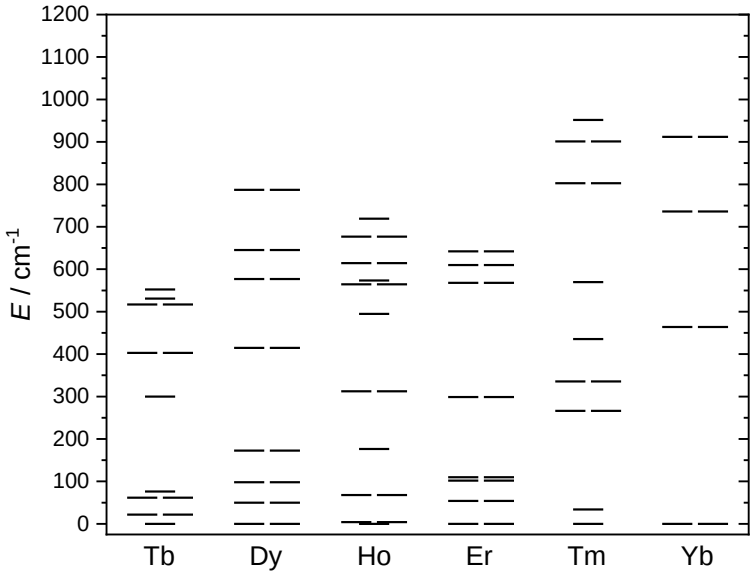

Figure S37 Energy level splitting of the ground multiplet in selected Ln(trensal) complexes. The values of Er(trensal)[3] and Yb(trensal)[4] are from literature. The energy level splitting of the remaining complexes are calculated using the CF parameters in Table S1.

Table S4 Energy levels (cm^{-1}) of selected Ln(trensal) complexes and **1**-**6**. The energy levels are determined as described in the figure text of Figure S36 and S37.

Tb(trensal)	Dy(trensal)	Ho(trensal)	Er(trensal)	Tm(trensal)	Yb(trensal)
0	0	0	0	0	0
22	0	4	0	34	0
22	50	4	54	266	464
62	50	68	54	266	464
62	98	68	102	335	736
76	98	176	102	335	736
300	173	312	110	435	912
403	173	312	110	569	912
403	414	495	299	803	
517	414	564	299	803	
517	577	564	568	901	
531	577	573	568	901	
552	645	615	610	952	
	645	615	610		
	787	677	642		
	787	677	642		
		719			
1	**2**	**3**	**4**	**5**	**6**
0	0	0	0	0	0
20	0	7	0	38	0
20	52	7	49	178	412
73	52	64	49	178	412
73	73	64	127	249	530
122	73	142	127	249	530
311	168	387	131	413	876
426	168	505	131	505	876
426	458	515	200	700	
552	458	515	200	700	
552	555	562	531	777	
626	555	562	531	777	
640	646	626	554	809	
	646	626	554		
	1068	656	567		
	1068	857	567		
		857			

Table S5 Eigenvector compositions of the energy levels (cm^{-1}) in the ground multiplet of **1**

E	0	20	20	73	73	122	311	426	426	552	552	626	640
|6>	2.0%	0.0%	0.0%	0.0%	0.0%	5.9%	7.3%	0.0%	0.0%	0.0%	0.0%	44.1%	40.7%
|5>	0.0%	6.3%	0.2%	12.6%	0.5%	0.0%	0.0%	0.0%	1.7%	78.0%	0.9%	0.0%	0.0%
|4>	0.0%	0.3%	14.2%	0.5%	13.7%	0.0%	0.0%	69.2%	1.4%	0.0%	0.6%	0.0%	0.0%
|3>	18.9%	0.0%	0.0%	0.0%	0.0%	43.9%	22.5%	0.0%	0.0%	0.0%	0.0%	5.9%	8.8%
|2>	0.0%	21.8%	0.5%	54.5%	2.0%	0.0%	0.0%	0.0%	0.7%	20.2%	0.2%	0.0%	0.0%
|1>	0.0%	1.4%	55.3%	0.6%	15.7%	0.0%	0.0%	26.4%	0.5%	0.0%	0.1%	0.0%	0.0%
|0>	58.2%	0.0%	0.0%	0.0%	0.0%	0.3%	40.4%	0.0%	0.0%	0.0%	0.0%	0.0%	1.0%
|-1>	0.0%	55.3%	1.4%	15.7%	0.6%	0.0%	0.0%	0.5%	26.4%	0.1%	0.0%	0.0%	0.0%
|-2>	0.0%	0.5%	21.8%	2.0%	54.5%	0.0%	0.0%	0.7%	0.0%	0.2%	20.2%	0.0%	0.0%
|-3>	18.9%	0.0%	0.0%	0.0%	0.0%	43.9%	22.5%	0.0%	0.0%	0.0%	0.0%	5.9%	8.8%
|-4>	0.0%	14.2%	0.3%	13.7%	0.5%	0.0%	0.0%	1.4%	69.2%	0.6%	0.0%	0.0%	0.0%
|-5>	0.0%	0.2%	6.3%	0.5%	12.6%	0.0%	0.0%	1.7%	0.0%	0.9%	78.0%	0.0%	0.0%
|-6>	2.0%	0.0%	0.0%	0.0%	0.0%	5.9%	7.3%	0.0%	0.0%	0.0%	0.0%	44.1%	40.7%

Table S6 Eigenvector compositions of the energy levels (cm^{-1}) in the ground multiplet of **2**

E	0	0	52	52	73	73	168	168	458	458	555	555	646	646	1068	1068
|15/2>	0.0%	0.0%	0.0%	1.3%	0.0%	0.0%	0.0%	0.0%	0.0%	7.8%	0.0%	0.0%	0.0%	0.0%	0.0%	90.8%
|13/2>	0.1%	10.5%	0.0%	0.0%	3.3%	0.0%	0.0%	47.7%	0.0%	0.0%	2.1%	0.0%	0.0%	36.3%	0.0%	0.0%
|11/2>	10.8%	0.1%	0.0%	0.0%	0.0%	46.4%	0.0%	0.0%	0.0%	0.0%	0.0%	41.5%	1.1%	0.0%	0.0%	0.0%
|9/2>	0.0%	0.0%	0.5%	37.0%	0.0%	0.0%	0.0%	0.0%	0.2%	53.9%	0.0%	0.0%	0.0%	0.0%	0.0%	8.4%
|7/2>	0.3%	25.0%	0.0%	0.0%	6.3%	0.0%	0.0%	13.0%	0.0%	0.0%	1.0%	0.0%	0.0%	54.3%	0.0%	0.0%
|5/2>	23.5%	0.3%	0.0%	0.0%	0.0%	20.8%	2.0%	0.0%	0.0%	0.0%	0.0%	49.5%	4.0%	0.0%	0.0%	0.0%
|3/2>	0.0%	0.0%	2.6%	58.6%	0.0%	0.0%	0.0%	0.0%	2.9%	35.2%	0.0%	0.0%	0.0%	0.0%	0.0%	0.7%
|1/2>	0.3%	29.2%	0.0%	0.0%	23.2%	0.0%	0.0%	37.2%	0.0%	0.0%	5.8%	0.0%	0.0%	4.3%	0.0%	0.0%
|-1/2>	29.2%	0.3%	0.0%	0.0%	0.0%	23.2%	37.2%	0.0%	0.0%	0.0%	0.0%	5.8%	4.3%	0.0%	0.0%	0.0%
|-3/2>	0.0%	0.0%	58.6%	2.6%	0.0%	0.0%	0.0%	0.0%	35.2%	2.9%	0.0%	0.0%	0.0%	0.0%	0.7%	0.0%
|-5/2>	0.3%	23.5%	0.0%	0.0%	20.8%	0.0%	0.0%	2.0%	0.0%	0.0%	49.5%	0.0%	0.0%	4.0%	0.0%	0.0%
|-7/2>	25.0%	0.3%	0.0%	0.0%	0.0%	6.3%	13.0%	0.0%	0.0%	0.0%	0.0%	1.0%	54.3%	0.0%	0.0%	0.0%
|-9/2>	0.0%	0.0%	37.0%	0.5%	0.0%	0.0%	0.0%	0.0%	53.9%	0.2%	0.0%	0.0%	0.0%	0.0%	8.4%	0.0%
|-11/2>	0.1%	10.8%	0.0%	0.0%	46.4%	0.0%	0.0%	0.0%	0.0%	0.0%	41.5%	0.0%	0.0%	1.1%	0.0%	0.0%
|-13/2>	10.5%	0.1%	0.0%	0.0%	0.0%	3.3%	47.7%	0.0%	0.0%	0.0%	0.0%	2.1%	36.3%	0.0%	0.0%	0.0%
|-15/2>	0.0%	0.0%	1.3%	0.0%	0.0%	0.0%	0.0%	0.0%	7.8%	0.0%	0.0%	0.0%	0.0%	0.0%	90.8%	0.0%

Table S7 Eigenvector compositions of the energy levels (cm^{-1}) in the ground multiplet of **3**

E	0	7	7	64	64	142	387	505	515	515	562	562	626	626	656	857	857
|8>	0.0%	0.0%	0.2%	0.0%	0.6%	0.0%	0.0%	0.0%	0.1%	2.1%	0.0%	0.5%	0.0%	0.2%	0.0%	0.0%	96.3%
|7>	0.0%	1.0%	0.0%	0.9%	0.0%	0.0%	0.0%	0.0%	18.7%	1.1%	68.3%	2.6%	7.4%	0.0%	0.0%	0.0%	0.0%
|6>	6.1%	0.0%	0.0%	0.0%	0.0%	19.7%	42.1%	29.4%	0.0%	0.0%	0.0%	0.0%	0.0%	0.0%	2.6%	0.0%	0.0%
|5>	0.0%	0.0%	19.4%	0.2%	37.2%	0.0%	0.0%	0.0%	1.7%	29.0%	0.2%	4.2%	0.0%	5.4%	0.0%	0.0%	2.8%
|4>	0.0%	34.4%	0.0%	26.1%	0.1%	0.0%	0.0%	0.0%	5.8%	0.3%	8.9%	0.3%	23.9%	0.0%	0.0%	0.0%	0.0%
|3>	31.6%	0.0%	0.0%	0.0%	0.0%	23.9%	4.8%	16.5%	0.0%	0.0%	0.0%	0.0%	0.0%	0.0%	23.3%	0.0%	0.0%
|2>	0.0%	0.0%	24.3%	0.1%	17.5%	0.0%	0.0%	0.0%	1.6%	26.6%	0.4%	10.3%	0.0%	18.4%	0.0%	0.0%	0.7%
|1>	0.0%	20.8%	0.0%	17.2%	0.1%	0.0%	0.0%	0.0%	12.2%	0.7%	4.1%	0.2%	44.6%	0.0%	0.0%	0.1%	0.0%
|0>	24.6%	0.0%	0.0%	0.0%	0.0%	12.8%	6.1%	8.3%	0.0%	0.0%	0.0%	0.0%	0.0%	0.0%	48.2%	0.0%	0.0%
|-1>	0.0%	0.0%	20.8%	0.1%	17.2%	0.0%	0.0%	0.0%	0.7%	12.2%	0.2%	4.1%	0.0%	44.6%	0.0%	0.0%	0.1%
|-2>	0.0%	24.3%	0.0%	17.5%	0.1%	0.0%	0.0%	0.0%	26.6%	1.6%	10.3%	0.4%	18.4%	0.0%	0.0%	0.7%	0.0%
|-3>	31.6%	0.0%	0.0%	0.0%	0.0%	23.9%	4.8%	16.5%	0.0%	0.0%	0.0%	0.0%	0.0%	0.0%	23.3%	0.0%	0.0%
|-4>	0.0%	0.0%	34.4%	0.1%	26.1%	0.0%	0.0%	0.0%	0.3%	5.8%	0.3%	8.9%	0.0%	23.9%	0.0%	0.0%	0.0%
|-5>	0.0%	19.4%	0.0%	37.2%	0.2%	0.0%	0.0%	0.0%	29.0%	1.7%	4.2%	0.2%	5.4%	0.0%	0.0%	2.8%	0.0%
|-6>	6.1%	0.0%	0.0%	0.0%	0.0%	19.7%	42.1%	29.4%	0.0%	0.0%	0.0%	0.0%	0.0%	0.0%	2.6%	0.0%	0.0%
|-7>	0.0%	0.0%	1.0%	0.0%	0.9%	0.0%	0.0%	0.0%	1.1%	18.7%	2.6%	68.3%	0.0%	7.4%	0.0%	0.0%	0.0%
|-8>	0.0%	0.2%	0.0%	0.6%	0.0%	0.0%	0.0%	0.0%	2.1%	0.1%	0.5%	0.0%	0.2%	0.0%	0.0%	96.3%	0.0%

Table S8 Eigenvector compositions of the energy levels (cm^{-1}) in the ground multiplet of **4**

E	0	0	49	49	127	127	131	131	200	200	531	531	554	554	567	567
|15/2>	0.0%	0.0%	0.4%	11.7%	0.0%	87.1%	0.0%	0.0%	0.0%	0.0%	0.0%	0.0%	0.0%	0.9%	0.0%	0.0%
|13/2>	1.8%	1.5%	0.0%	0.0%	0.0%	0.0%	11.1%	1.0%	0.1%	71.5%	0.3%	8.6%	0.0%	0.0%	2.1%	1.9%
|11/2>	1.9%	2.3%	0.0%	0.0%	0.0%	0.0%	4.3%	45.3%	9.5%	0.0%	12.2%	0.4%	0.0%	0.0%	11.5%	12.6%
|9/2>	0.0%	0.0%	2.6%	40.7%	1.2%	4.4%	0.0%	0.0%	0.0%	0.0%	0.0%	0.0%	1.8%	49.3%	0.0%	0.0%
|7/2>	19.2%	16.4%	0.0%	0.0%	0.0%	0.0%	4.4%	0.4%	0.0%	4.2%	1.5%	41.4%	0.0%	0.0%	6.6%	6.0%
|5/2>	14.1%	16.5%	0.0%	0.0%	0.0%	0.0%	1.2%	12.9%	4.1%	0.0%	26.9%	1.0%	0.0%	0.0%	11.1%	12.2%
|3/2>	0.0%	0.0%	7.4%	37.3%	1.9%	5.4%	0.0%	0.0%	0.0%	0.0%	0.0%	0.0%	5.4%	42.6%	0.0%	0.0%
|1/2>	14.2%	12.1%	0.0%	0.0%	0.0%	0.0%	17.8%	1.7%	0.0%	10.6%	0.3%	7.3%	0.0%	0.0%	18.8%	17.1%
|-1/2>	12.1%	14.2%	0.0%	0.0%	0.0%	0.0%	1.7%	17.8%	10.6%	0.0%	7.3%	0.3%	0.0%	0.0%	17.1%	18.8%
|-3/2>	0.0%	0.0%	37.3%	7.4%	5.4%	1.9%	0.0%	0.0%	0.0%	0.0%	0.0%	0.0%	42.6%	5.4%	0.0%	0.0%
|-5/2>	16.5%	14.1%	0.0%	0.0%	0.0%	0.0%	12.9%	1.2%	0.0%	4.1%	1.0%	26.9%	0.0%	0.0%	12.2%	11.1%
|-7/2>	16.4%	19.2%	0.0%	0.0%	0.0%	0.0%	0.4%	4.4%	4.2%	0.0%	41.4%	1.5%	0.0%	0.0%	6.0%	6.6%
|-9/2>	0.0%	0.0%	40.7%	2.6%	4.4%	1.2%	0.0%	0.0%	0.0%	0.0%	0.0%	0.0%	49.3%	1.8%	0.0%	0.0%
|-11/2>	2.3%	1.9%	0.0%	0.0%	0.0%	0.0%	45.3%	4.3%	0.0%	9.5%	0.4%	12.2%	0.0%	0.0%	12.6%	11.5%
|-13/2>	1.5%	1.8%	0.0%	0.0%	0.0%	0.0%	1.0%	11.1%	71.5%	0.1%	8.6%	0.3%	0.0%	0.0%	1.9%	2.1%
|-15/2>	0.0%	0.0%	11.7%	0.4%	87.1%	0.0%	0.0%	0.0%	0.0%	0.0%	0.0%	0.0%	0.9%	0.0%	0.0%	0.0%

Table S9 Eigenvector compositions of the energy levels (cm^{-1}) in the ground multiplet of **5**

E	0	38	178	178	249	249	413	505	700	700	777	777	809
|6>	31.2%	37.7%	0.0%	0.0%	0.0%	0.0%	18.8%	11.7%	0.0%	0.0%	0.0%	0.0%	0.7%
|5>	0.0%	0.0%	33.4%	12.0%	2.9%	7.9%	0.0%	0.0%	0.8%	41.5%	1.1%	0.4%	0.0%
|4>	0.0%	0.0%	2.9%	8.2%	44.0%	16.1%	0.0%	0.0%	0.9%	0.0%	7.2%	20.7%	0.0%
|3>	18.1%	10.1%	0.0%	0.0%	0.0%	0.0%	28.9%	22.9%	0.0%	0.0%	0.0%	0.0%	20.0%
|2>	0.0%	0.0%	30.4%	10.9%	0.4%	1.1%	0.0%	0.0%	0.7%	36.8%	14.6%	5.1%	0.0%
|1>	0.0%	0.0%	0.6%	1.6%	20.3%	7.4%	0.0%	0.0%	18.8%	0.4%	13.1%	37.7%	0.0%
|0>	1.5%	4.4%	0.0%	0.0%	0.0%	0.0%	4.6%	30.9%	0.0%	0.0%	0.0%	0.0%	58.6%
|-1>	0.0%	0.0%	1.6%	0.6%	7.4%	20.3%	0.0%	0.0%	0.4%	18.8%	37.7%	13.1%	0.0%
|-2>	0.0%	0.0%	10.9%	30.4%	1.1%	0.4%	0.0%	0.0%	36.8%	0.7%	5.1%	14.6%	0.0%
|-3>	18.1%	10.1%	0.0%	0.0%	0.0%	0.0%	28.9%	22.9%	0.0%	0.0%	0.0%	0.0%	20.0%
|-4>	0.0%	0.0%	8.2%	2.9%	16.1%	44.0%	0.0%	0.0%	0.0%	0.9%	20.7%	7.2%	0.0%
|-5>	0.0%	0.0%	12.0%	33.4%	7.9%	2.9%	0.0%	0.0%	41.5%	0.8%	0.4%	1.1%	0.0%
|-6>	31.2%	37.7%	0.0%	0.0%	0.0%	0.0%	18.8%	11.7%	0.0%	0.0%	0.0%	0.0%	0.7%

Table S10 Eigenvector compositions of the energy levels (cm^{-1}) in the ground multiplet of **6**

E	0	0	412	412	530	530	876	876
|7/2>	48.4%	0.2%	28.1%	8.8%	0.0%	0.0%	0.0%	14.5%
|5/2>	0.1%	19.4%	13.1%	41.9%	0.0%	0.0%	25.5%	0.0%
|3/2>	0.0%	0.0%	0.0%	0.0%	0.4%	99.6%	0.0%	0.0%
|1/2>	31.8%	0.1%	6.1%	1.9%	0.0%	0.0%	0.0%	60.0%
|-1/2>	0.1%	31.8%	1.9%	6.1%	0.0%	0.0%	60.0%	0.0%
|-3/2>	0.0%	0.0%	0.0%	0.0%	99.6%	0.4%	0.0%	0.0%
|-5/2>	19.4%	0.1%	41.9%	13.1%	0.0%	0.0%	0.0%	25.5%
|-7/2>	0.2%	48.4%	8.8%	28.1%	0.0%	0.0%	14.5%	0.0%

Ac susceptibility

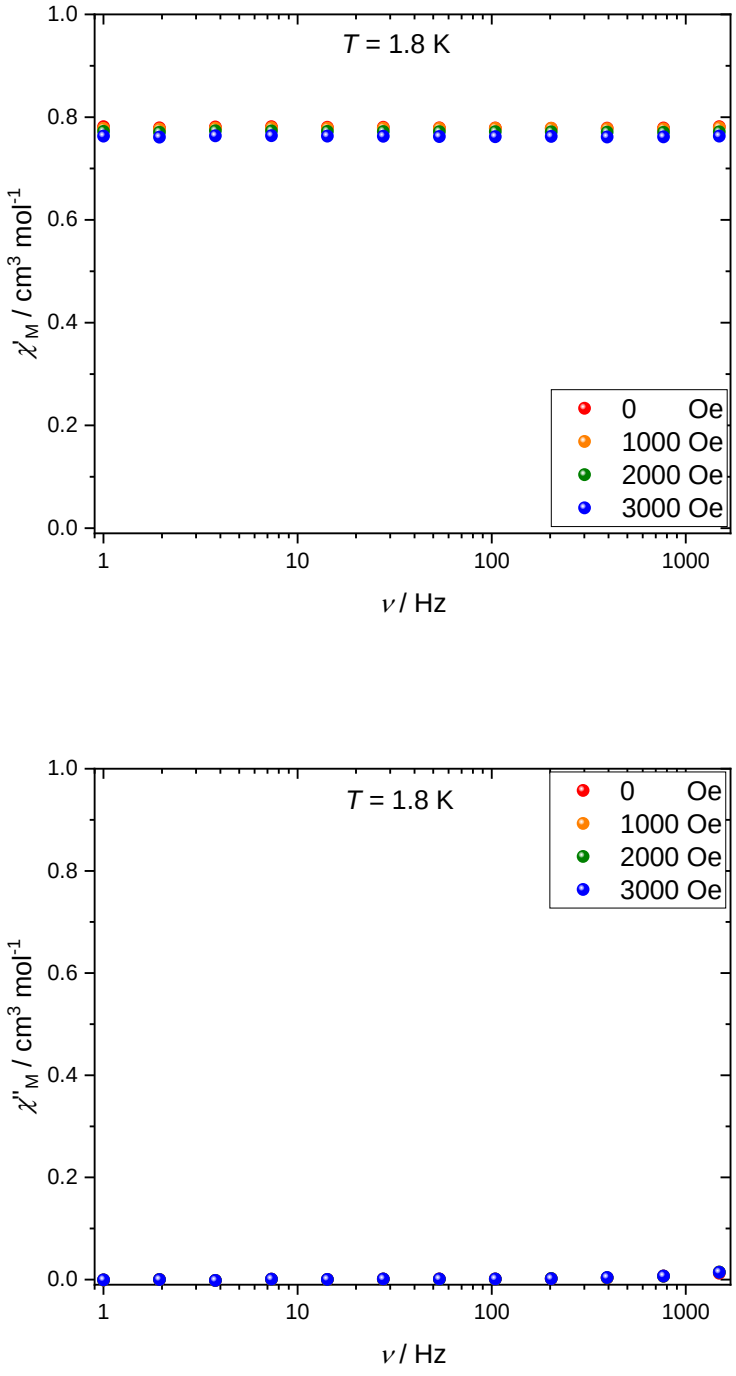

Figure S38 In-phase (top) and out-of-phase (bottom) ac susceptibility response of **1** in the frequency range 1-1500 Hz at varying static magnetic fields.

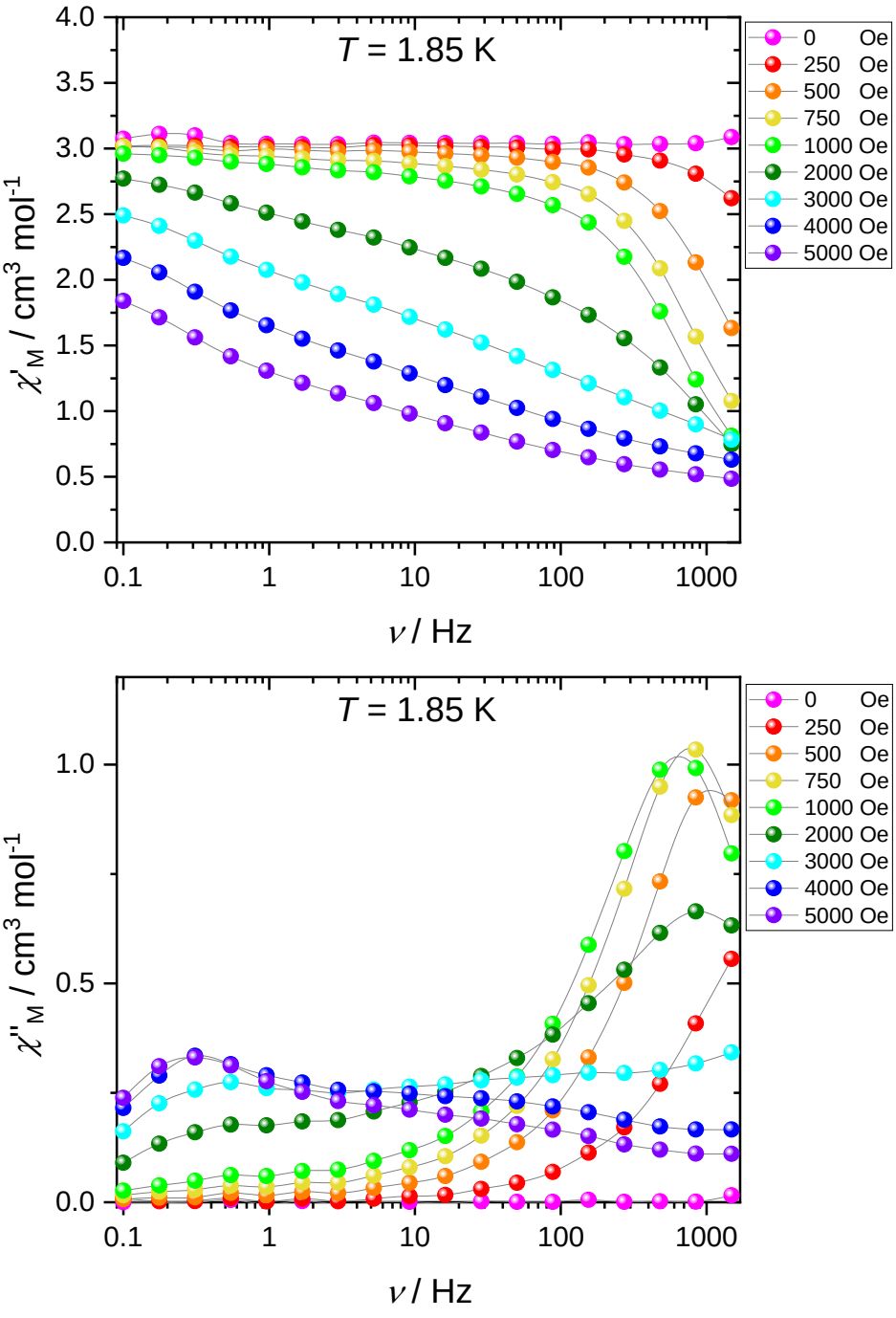

Figure S39 In-phase (top) and out-of-phase (bottom) ac susceptibility response of **2** in the frequency range 0.1-1500 Hz at varying static magnetic fields. Solid lines are guidelines for the eye.

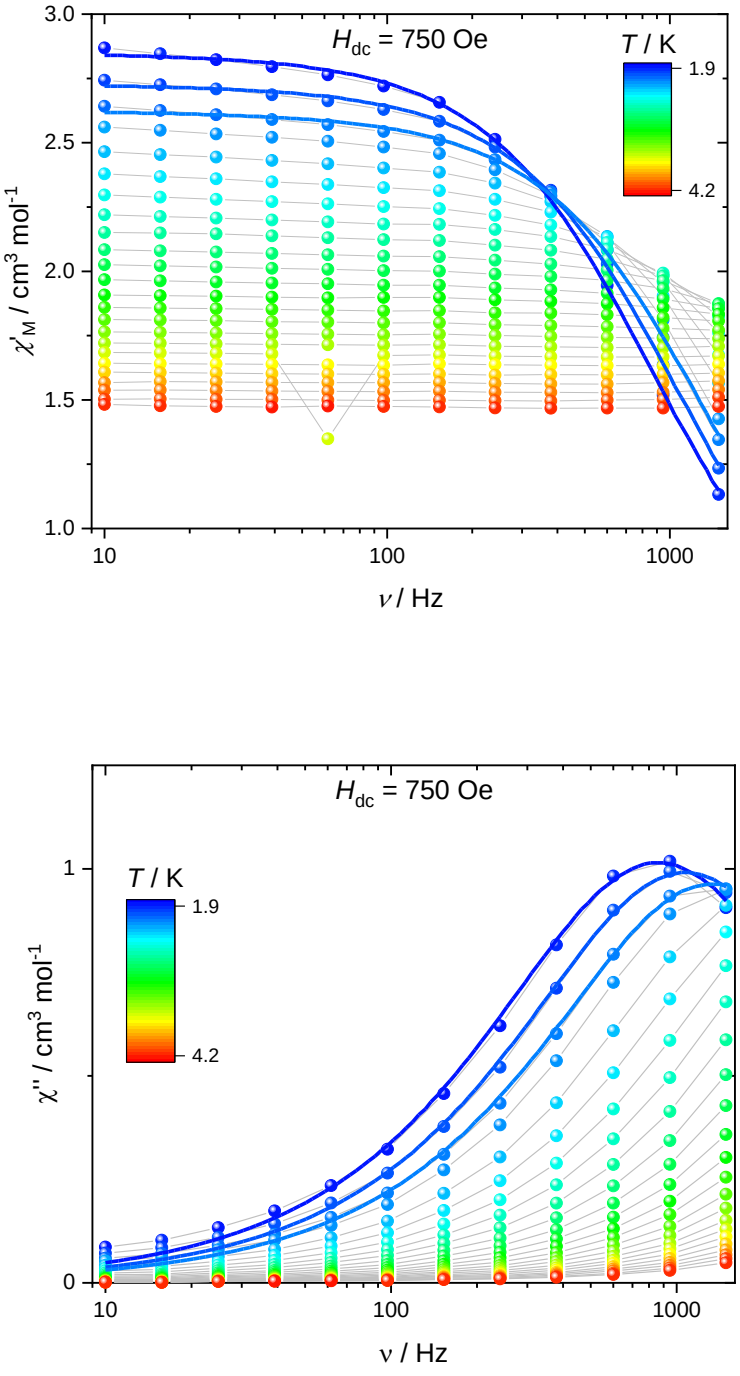

Figure S40 Temperature dependence of the in-phase (top) and out-of-phase (bottom) ac susceptibility response of **2** in the frequency range 10-1500 Hz under an applied static magnetic field of 750 Oe. Grey lines are guidelines for the eye while the colored lines are fits to a generalised Debye model as described in the main text.

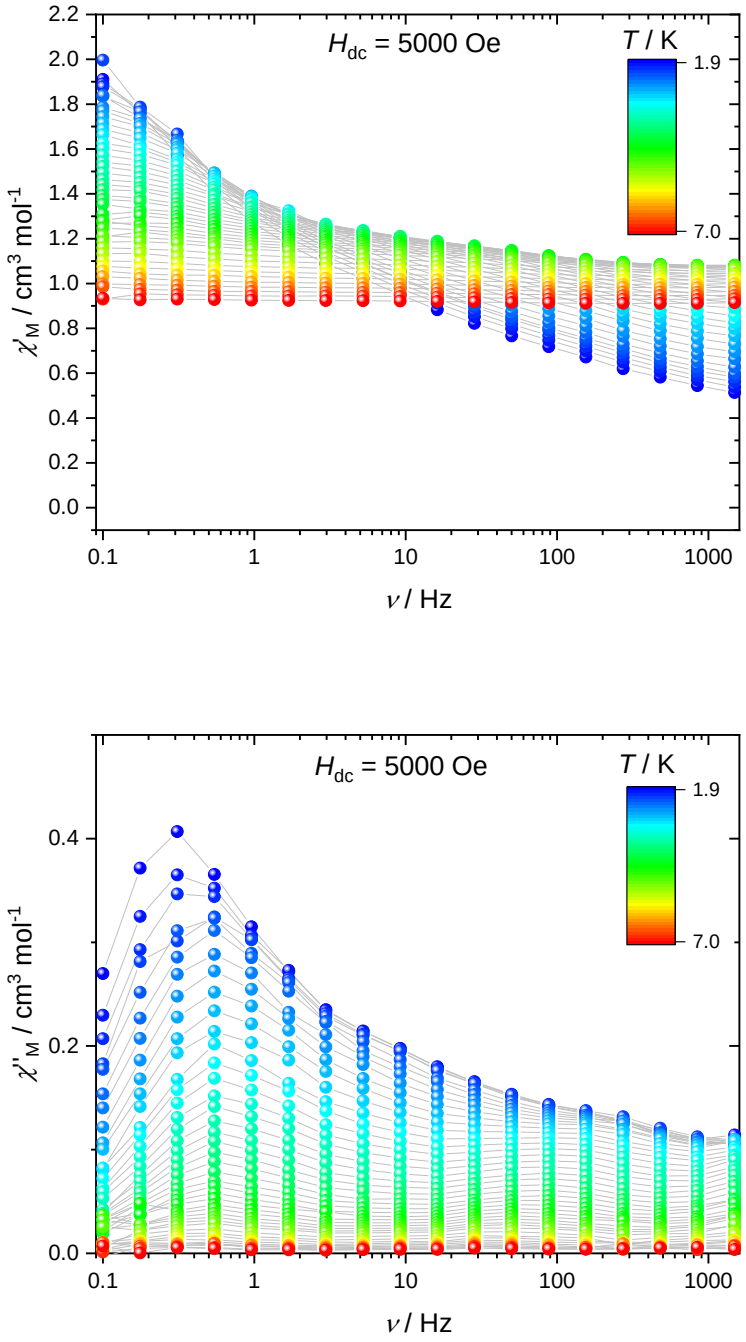

Figure S41 Temperature dependence of the in-phase (top) and out-of-phase (bottom) ac susceptibility response of **2** in the frequency range 0.1-1500 Hz under an applied static magnetic field of 5000 Oe. Solid lines are guidelines for the eye.

Table S11 Relaxation times and α parameters extracted by fitting a generalised Debye model to the ac susceptibility data of **2** measured under an applied field of 750 Oe.

Temp / K	τ **/ ms**	**α**
1.9	0.185	0.125
2.0	0.149	0.119
2.1	0.119	0.123

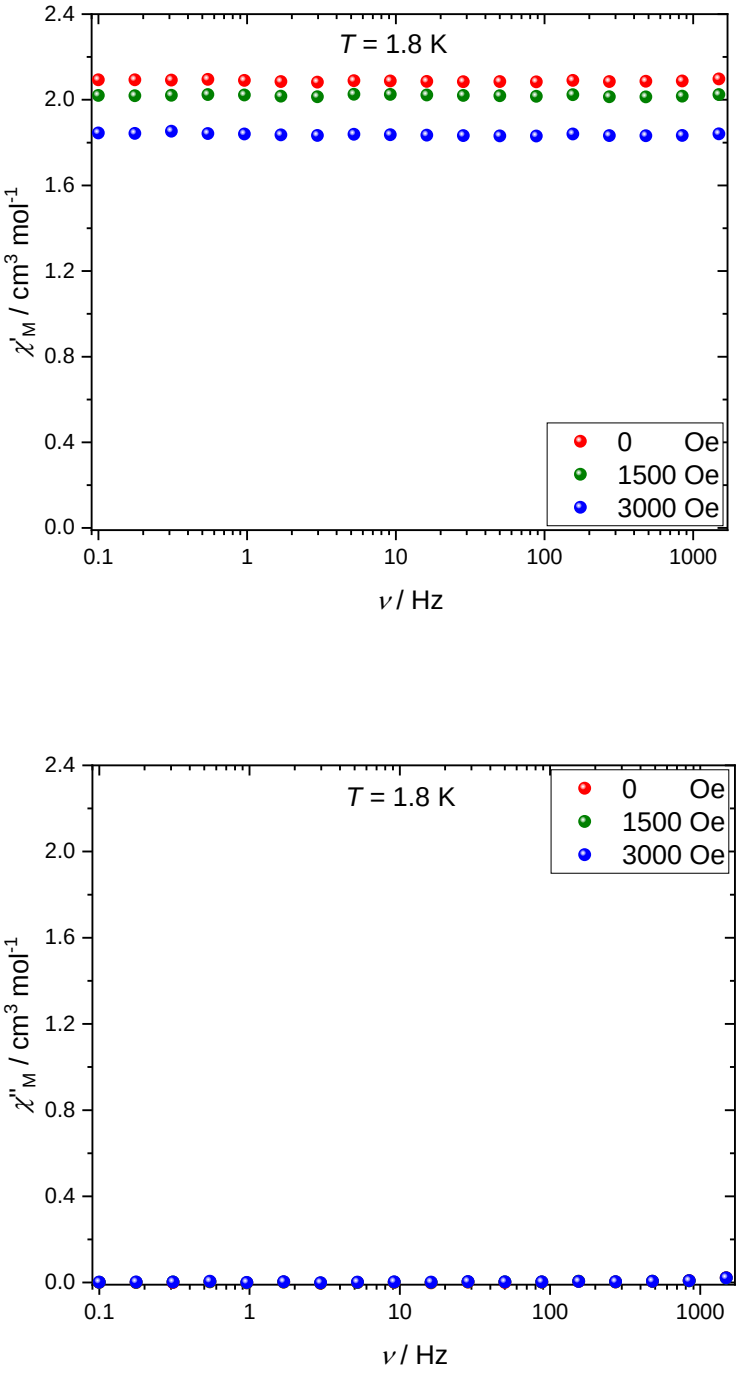

Figure S42 In-phase (top) and out-of-phase (bottom) ac susceptibility response of **3** in the frequency range 0.1-1500 Hz at varying static magnetic fields.

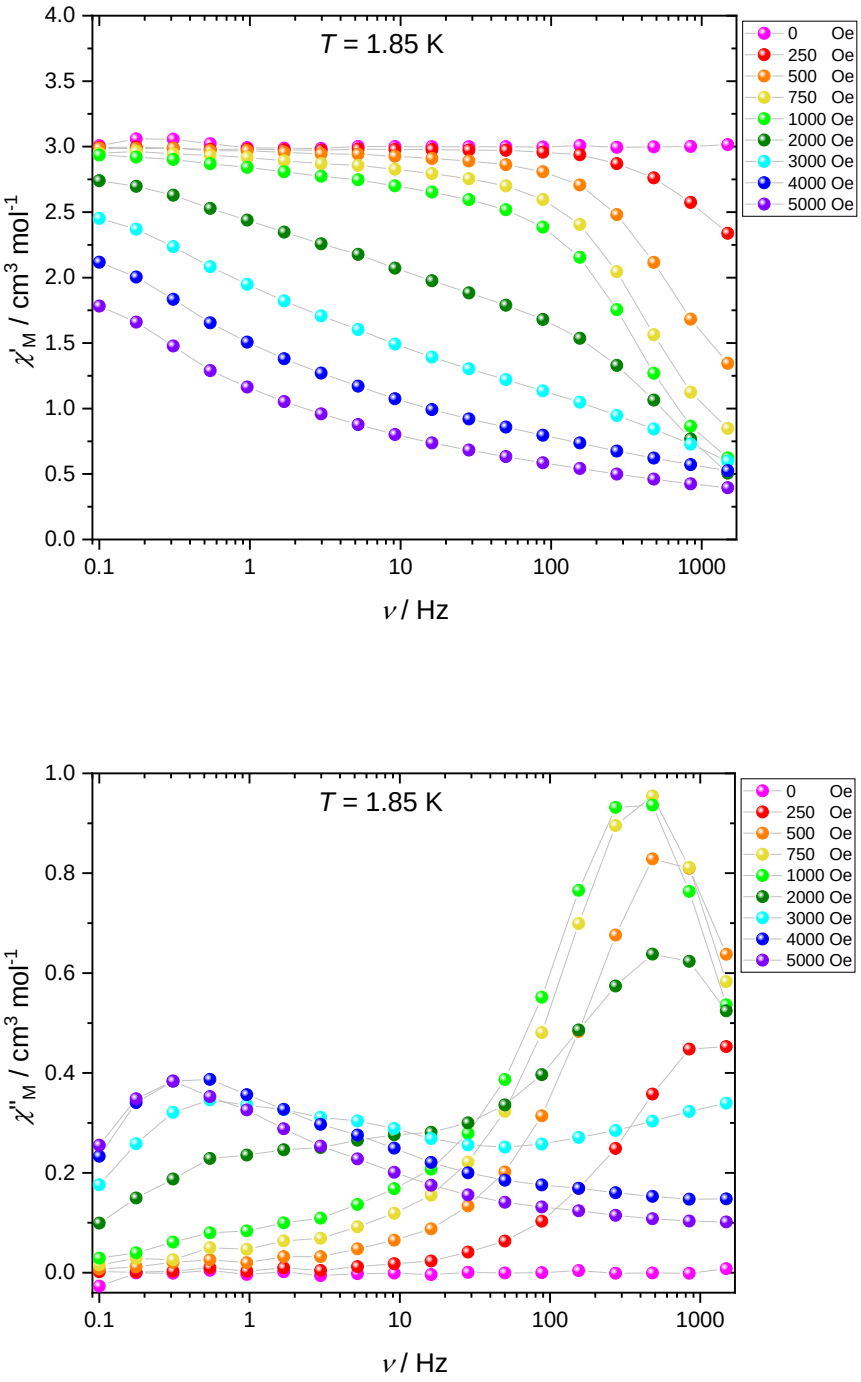

Figure S43 In-phase (top) and out-of-phase (bottom) ac susceptibility response of **4** in the frequency range 0.1-1500 Hz at varying static magnetic fields. Solid lines are guidelines for the eye.

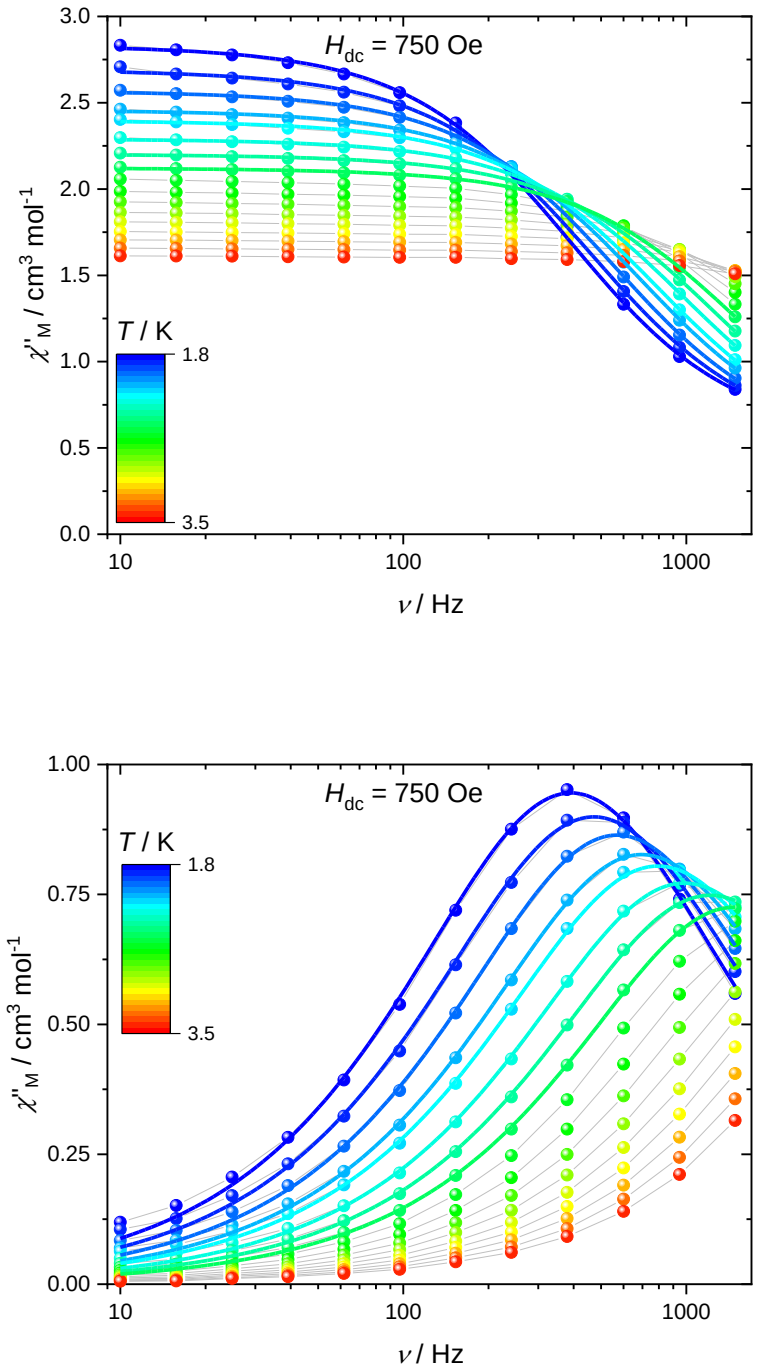

Figure S44 Temperature dependence of the in-phase (top) and out-of-phase (bottom) ac susceptibility response of **4** in the frequency range 10-1500 Hz under an applied static magnetic field of 750 Oe. Grey lines are guidelines for the eye while the colored lines are fits to a generalised Debye model as described in the main text.

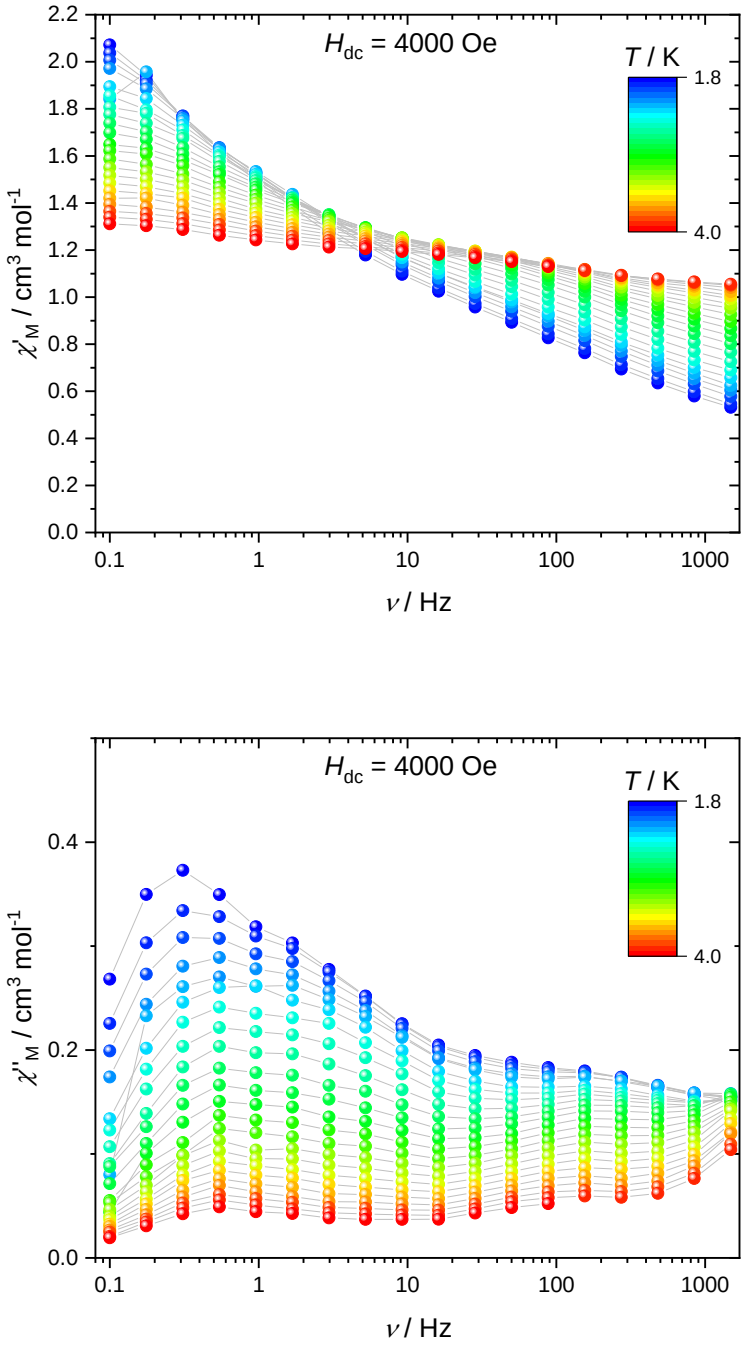

Figure S45 Temperature dependence of the in-phase (top) and out-of-phase (bottom) ac susceptibility response of **4** in the frequency range 0.1-1500 Hz under an applied static magnetic field of 4000 Oe. Grey lines are guidelines for the eye.

Table S12 Relaxation times and α parameters extracted by fitting a generalised Debye model to the ac susceptibility data of **4** measured under an applied field of 750 Oe.

Temp / K	**τ / ms**	**α**
1.8	0.407	0.121
1.9	0.338	0.120
2.0	0.279	0.114
2.1	0.229	0.114
2.2	0.200	0.118
2.3	0.162	0.112
2.4	0.131	0.110
2.5	0.107	0.107

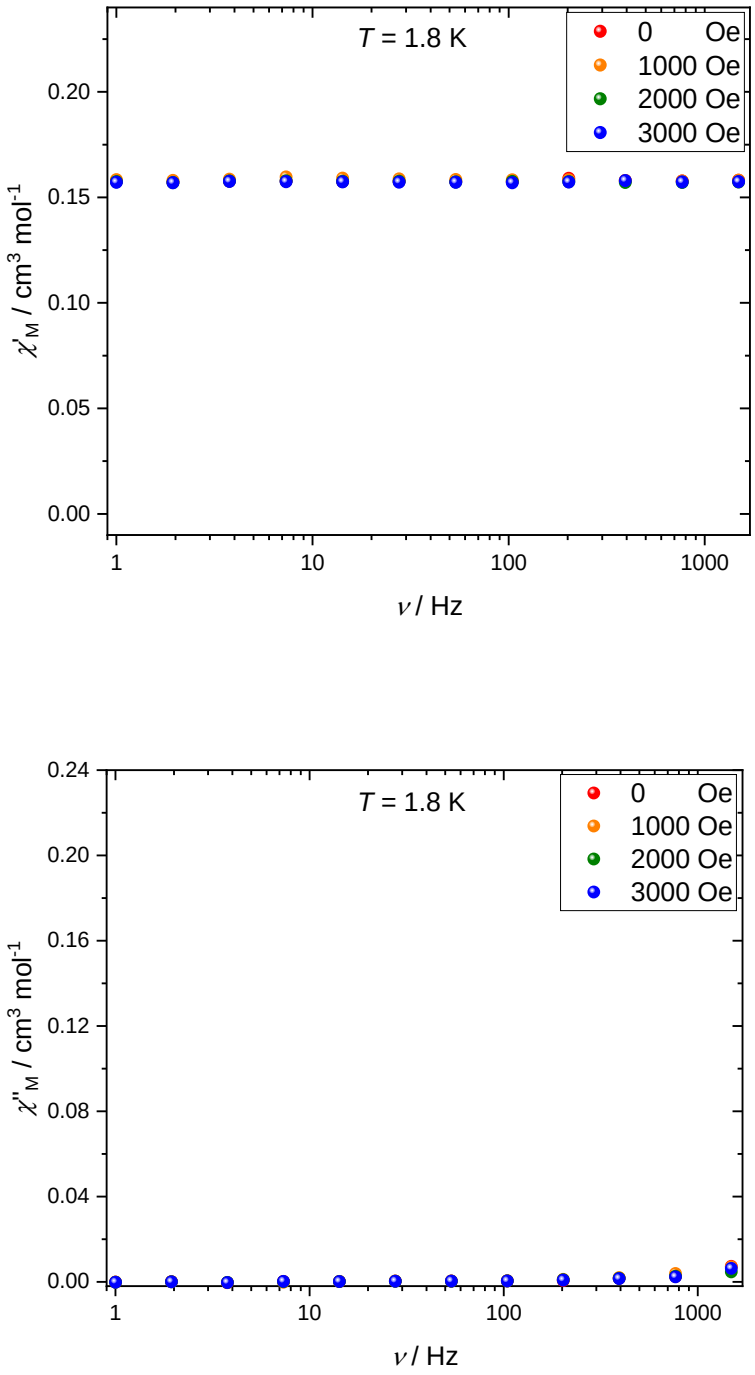

Figure S46 In-phase (top) and out-of-phase (bottom) ac susceptibility response of **5** in the frequency range 1-1500 Hz at varying static magnetic fields.

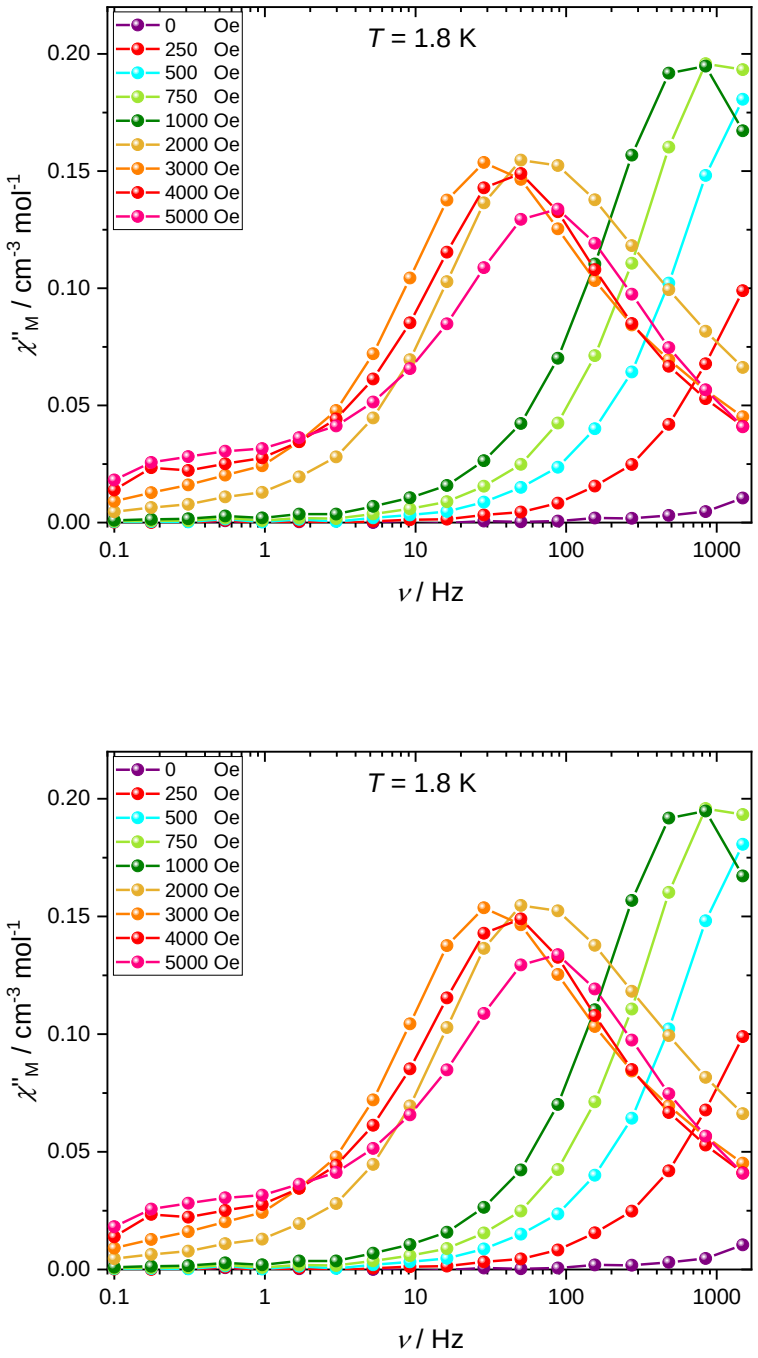

Figure S47 In-phase (top) and out-of-phase (bottom) ac susceptibility response of **6** in the frequency range 0.1-1500 Hz at varying static magnetic fields. Solid lines are guidelines for the eye.

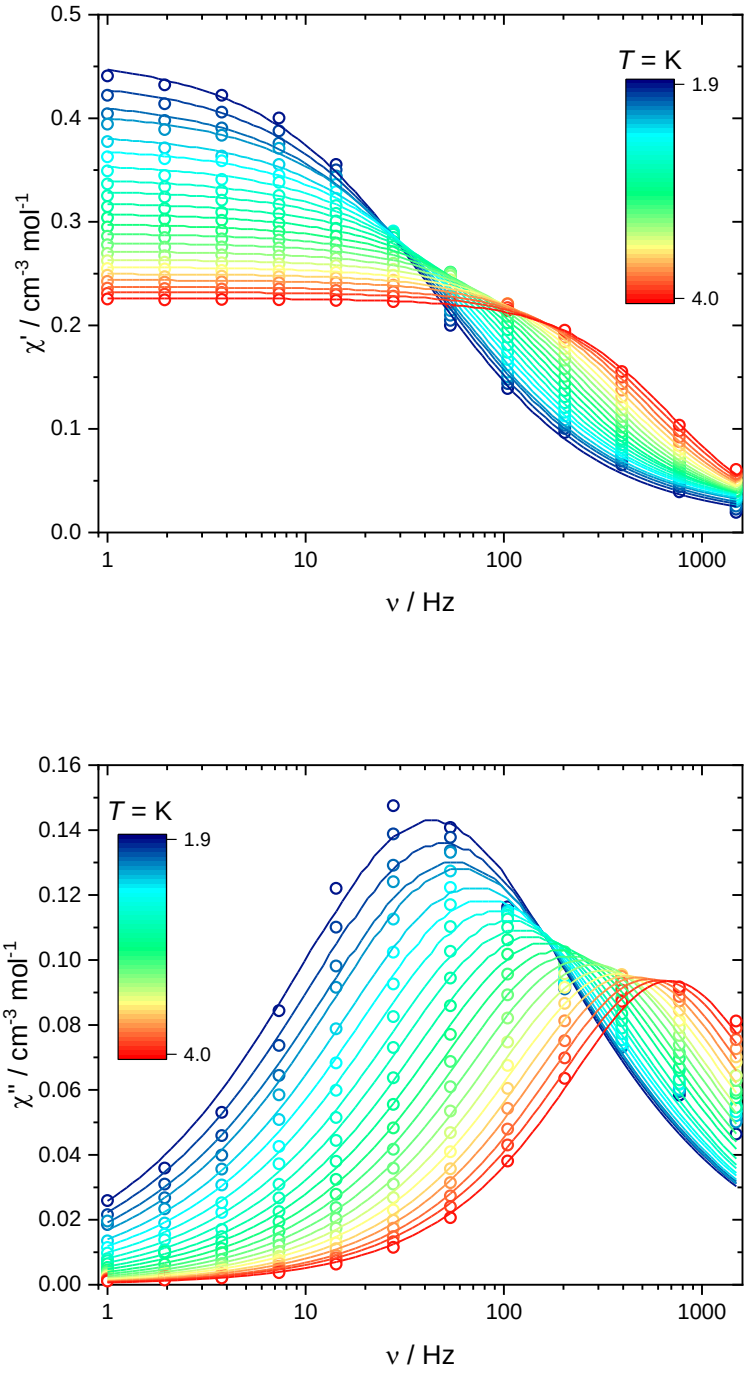

Figure S48 Temperature dependence of the in-phase (top) and out-of-phase (bottom) ac susceptibility response of **6** in the frequency range 1-1500 Hz under an applied static magnetic field of 3000 Oe. Colored lines are fits to a generalised Debye model as described in the main text.

Table S13 Relaxation times and α parameters extracted by fitting a generalised Debye model to the ac susceptibility data of **6** measured under an applied field of 3000 Oe.

Temp / K	τ / ms	α
1.9	3.66	0.284
2.0	3.22	0.282
2.1	2.84	0.278
2.2	2.64	0.264
2.3	2.26	0.258
2.4	1.98	0.251
2.5	1.73	0.240
2.6	1.49	0.230
2.7	1.32	0.219
2.8	1.14	0.209
2.9	0.980	0.205
3.0	0.851	0.196
3.1	0.742	0.186
3.2	0.643	0.178
3.3	0.558	0.170
3.4	0.496	0.161
3.5	0.430	0.157
3.6	0.380	0.144
3.7	0.335	0.136
3.8	0.296	0.125
3.9	0.259	0.127
4.0	0.232	0.114

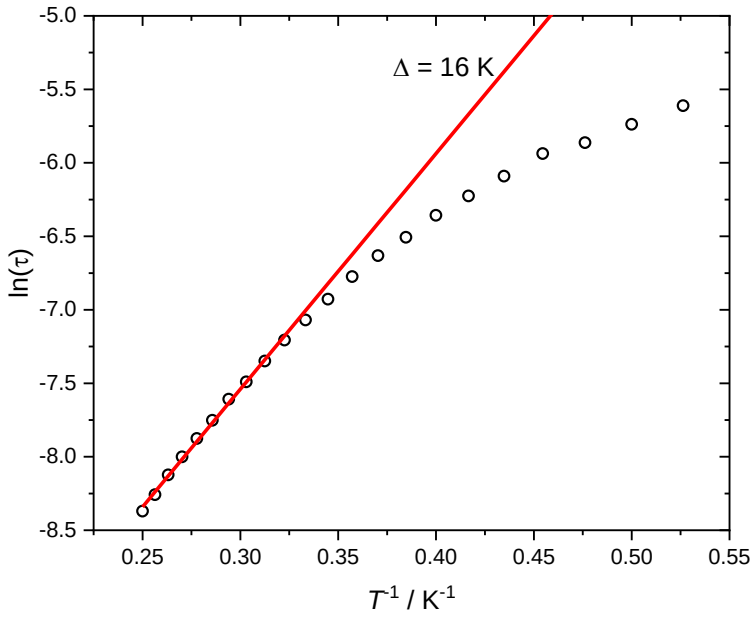

Figure S49 Relaxation times (τ) obtained for **6** by fitting the ac susceptibility to the generalised Debye model described in the main text. The red line is a fit to an Arrhnius function.

Preparation from MeCN

Synthesis of 4

DFMP (0.40 g; 2.4 mmol) and $Er(OTf)_3 \cdot 6H_2O$ (0.57 g; 0.79 mmol) were dissolved in hot MeCN (150 ml). To this was added dropwise a solution of tren (0.23 g; 1.6 mmol) in MeOH (25 ml) over 45 min. The solution was then boiled for 1 hour while being reduced to a volume of ca. 150 ml. Then a solution of Et_3N (0.4 ml; 3 mmol) in MeCN (10 ml) was added slowly. The orange solution was then left for a week at room temperature producing a yellow precipitate. This was isolated and washed 3 times with EtOH and 3 times with diethyl ether.

Yield: 0.35 g (47 %). Anal. Calcd. for $C_{39}H_{53}N_8O_7Er$: C, 51.30; H, 5.85; N, 12.27. Found: C, 51.56; H, 5.59; N, 12.26.

5 was prepared analogously. Yield: 0.32 g (42 %). Anal. Calcd. for $C_{39}H_{53}N_8O_7Tm$: C, 51.20; H, 5.84; N, 12.25. Found: C, 51.33; H, 5.55; N, 12.15.

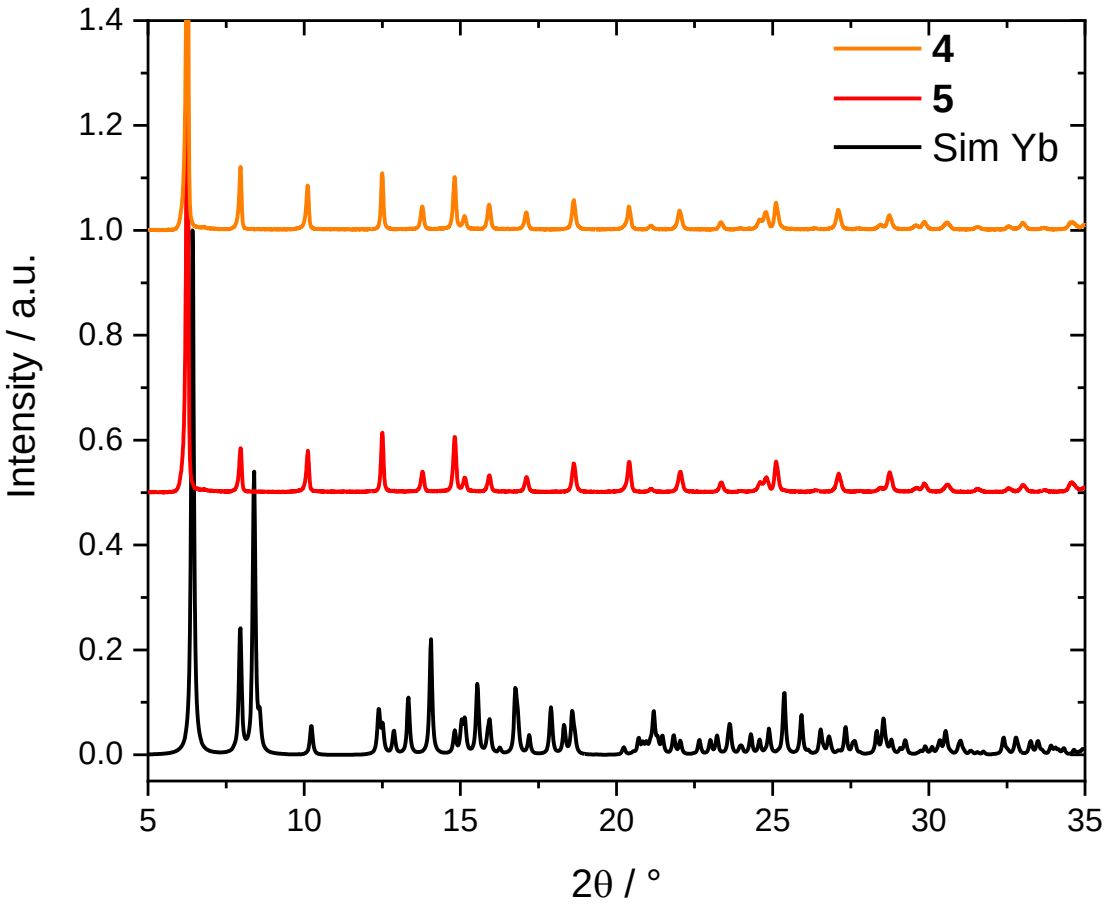

Figure S50 PXRD of **4** and **5** prepared from MeCN instead of MeCN/$CHCl_3$**.** The simulation is based on a crystal structure of **6** (prepared from a MeCN/$CHCl_3$ mixture) measured at room temperature.

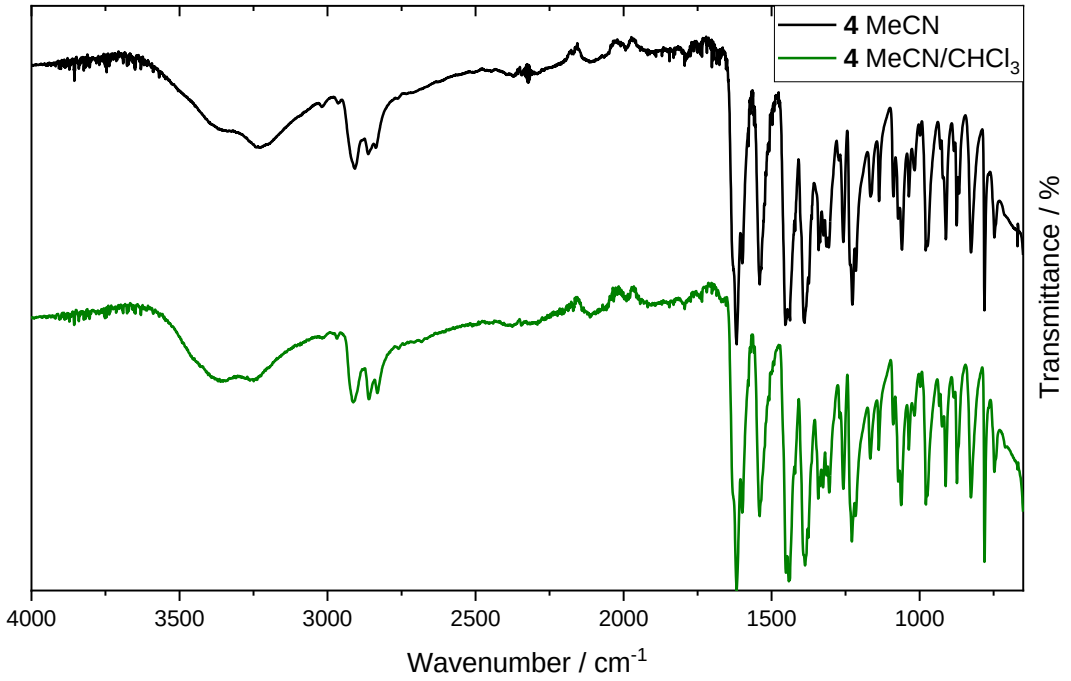

Figure S51 Comparison of IR spectra of **4** prepared from MeCN or MeCN/$CHCl_3$

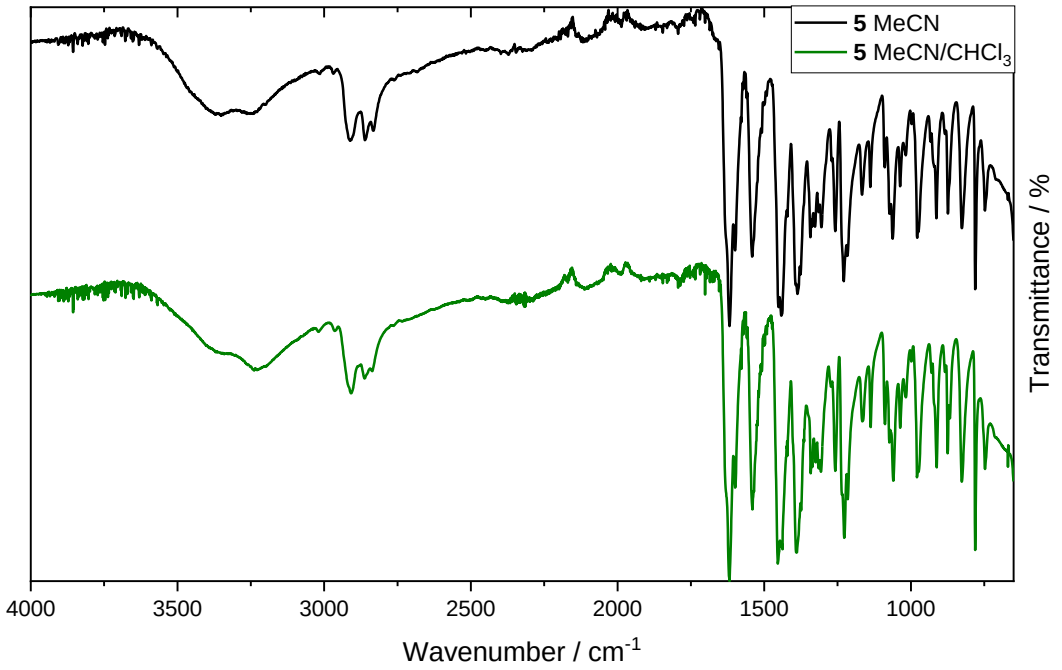

Figure S52 Comparison of IR spectra of **5** prepared from MeCN or MeCN/$CHCl_3$.

1. H. E. Gottlieb, V. Kotlyar and A. Nudelman, *J Org Chem*, 1997, **62**, 7512-7515.
2. B. M. Flanagan, P. V. Bernhardt, E. R. Krausz, S. R. Luthi and M. J. Riley, *Inorg Chem*, 2002, **41**, 5024-5033.
3. B. M. Flanagan, P. V. Bernhardt, E. R. Krausz, S. R. Luthi and M. J. Riley, *Inorg Chem*, 2001, **40**, 5401-5407.
4. K. S. Pedersen, J. Dreiser, H. Weihe, R. Sibille, H. V. Johannesen, M. A. Sorensen, B. E. Nielsen, M. Sigrist, H. Mutka, S. Rols, J. Bendix and S. Piligkos, *Inorg Chem*, 2015, **54**, 7600-7606.
5. A. Abragam and B. Bleaney, *Electron Paramagnetic Resonance of Transition Ions*, Dover, 1986.
6. in *Handbook on the Physics and Chemistry of Rare Earths*, Elsevier, 1996, vol. 23, ch. 155.